A physics-informed machine learning framework for strength prediction, uncertainty quantification, and optimization of chemically stabilized soils

Ajay Pratap Singh Rathor[1*]

[1] *Department of Civil Engineering, Rajasthan Technical University, Kota, Rajasthan, India*

Email: apsrathor.phd19@rtu.ac.in

ORCID: 0000-0002-7085-1690

Abdollah Tabaroei[2*]

[2] *Department of Civil Engineering, Eshragh Institute of Higher Education, Bojnourd, Iran*

* Corresponding author: Abdollah Tabaroei, a.tabaroei@eshragh.ac.ir

ORCID: 0000-0002-1324-2397

Arindam Dey[3]

[3]*Department of Civil Engineering, Indian Institute of Technology, Guwahati, India*

[3]*Center for Disaster Management and Research (CDMR), IIT Guwahati*

Email: arindam.dey@iitg.ac.in

ORCID: 0000-0001-7007-2729

Jitendra Kumar Sharma[4]

[4]*Department of Civil Engineering, Rajasthan Technical University, Kota, Rajasthan, India*

Email: jksharma@rtu.ac.in

ORCID: 0000-0002-4584-6793

Abstract

When it comes to enhancing subgrade soils, the most common approach is chemical stabilization. However, predicting unconfined compressive strength (UCS) of stabilized soils is often complicated due to the numerous complex nonlinear relationships present. There are numerous factors that can influence the relationships such as the soil properties, binder chemistry, alkaline activators, water content, and curing conditions. Most of the existing predictive models have limitations such as focusing on only specific types of materials, lack of transparency and neglecting uncertainty, which directly limits engineering design applications. The purpose of this study is to provide a unique datadriven and physics informed framework for UCS prediction, interpretation, uncertainty quantification and the ultimate optimization of mixture design. The first of its kind, this study incorporates a thoroughly curated dataset of 990 laboratory mixtures which featured unique varieties of soil, industrial by products, alkaline activators and nano-additives of different curing durations. Various machine learning models including linear regression, random forests, support vector regression, gradient boosting and artificial neural networks (ANN) were tested. Out of the models tested, the ANN produced the best results with an R^2 value of 0.919 and RMSE of 1.124 MPa. A physics-informed neural network (PINN) was further developed to enforce physically consistent trends, providing improved interpretability despite marginally reduced accuracy.

Reliability based UCS estimation was possible as predictive uncertainty was quantified using monte carlo simulation. Along with defined geo-chemistry principles, SHAP analysis identified the three most important controlling factors to be curing time, GGBS content, and alkaline activators. A multi-objective optimization framework revealed the possible design of economically viable and environmentally friendly stabilization mixes. The developed framework represents a real-world decision making support system for geo-stabilization.

Keywords: Soil stabilization, ANN, Monte Carlo simulation, SHAP Analysis, Sustainable Construction

Nomenclature

Geotechnical Index Properties

Plastic limit (%)	Plastic Limit of soil (Atterberg limit)
Liquid limit (%)	Liquid Limit of soil
Water content (%)	Natural Water Content
sand	Percentage of sand fraction (%)
silt	Percentage of silt fraction (%)
clay	Percentage of clay fraction (%)

Chemical Oxides (Soil / Binder Composition)

SiO_2	Silica content (%)
Al_2O_3	Alumina content (%)
CaO	Calcium oxide (%)
Fe_2O_3	Ferric oxide (%)
MgO	Magnesium oxide (%)

Alkali Activation Variables

NaOH	Sodium hydroxide molarity / % content
NS-Na_2O	Sodium oxide content in sodium silicate
NS-SiO_2	Silica content in sodium silicate
Curing time	Curing duration for treated soil (days)

Binder / Additive Content (% by weight)

Mix_BA_percent	Bagasse Ash (%)
Mix_CS_percent	Corn Straw Ash / Cement Slurry (%)
Mix_Ca_percent	Calcium additive (%)
Mix_CaO_percent	Calcium oxide additive (%)
Mix_EA_percent	Eggshell Ash (%)
Mix_FA_percent	Fly Ash (%)
Mix_GGBS_percent	Ground Granulated Blast Furnace Slag (%)

Mix_GP_percent	Granite Powder (%)
Mix_MK_percent	Metakaolin (%)
Mix_MP_percent	Marble Powder (%)
Mix_MgO_percent	Magnesium oxide additive (%)
Mix_NS_percent	Sodium Silicate (%)
Mix_NaOH_percent	Sodium Hydroxide (%)
Mix_POFA_percent	Palm Oil Fuel Ash (%)
Mix_Quicklime_percent	Quicklime (%)
Mix_RHA_percent	Rice Husk Ash (%)
Mix_RHAA_percent	Activated Rice Husk Ash (%)
Mix_SF_percent	Silica Fume (%)
Mix_Slag_percent	Slag (%)
Mix_VA_percent	Volcanic Ash (%)
Mix_w_percent	Water-to-binder ratio (%)
Mix_water_percent	Added water content (%)

1. Introduction

The global construction industry is under increasing pressure to develop sustainable construction practices, including utilizing locally available soils and industrial by-products. Growing demand for infrastructure development all over the world, coupled with the dire need to adhere to sustainable construction, has put a sharp focus on techniques of ground improvement [1, 2]. One of the vital issues in civil engineering involves the construction of stable foundations, pavements, and embankments using soft or expansive soils and characterized by low shear strength, high compressibility, and poor durability [3, 4]. So far, the chemical stabilization of such problematic soils has proven to be an effective and popular method for enhancing their engineering properties [5, 6]. This process involves the introduction of binders or chemical agents into the soil, which, through the induced reactions, improve strength and reduce permeability and swell-shrink potential [7].

Traditionally, OPC and lime have been the main binders used for soil stabilization [8-10]. However, OPC production is very energy-intensive and alone accounts for about 5-8% of total anthropogenic CO_2 emissions globally [11, 12]. This significant environmental issue has, therefore, driven the search for sustainable alternatives. This has resulted in the prolific investigation of industrial by-products, including GGBS, FA, and SF, among others [13, 14]. Besides lowering the carbon footprint for the stabilization projects, these materials mostly exhibit excellent pozzolanic or latent hydraulic properties upon proper activation [15, 16]. The activation, which is normally done with alkaline solutions such as sodium hydroxide or sodium silicate, is an important step in the dissolution of silica and alumina from the soil and by-products and forms cementitious gels, including C-S-H and C-A-S-H [17, 18]. Nano-materials,

especially NS, have recently demonstrated potential for further accelerating the pozzolanic reactions and refining the pore structure of the stabilized soils, thereby contributing to significant early and long-term strength gains [19, 20]. However, the effectiveness of any stabilization scheme is influenced by a number of interlinked factors. These include, but are not limited to, the intrinsic properties of the soil itself, such as mineralogy, particle size distribution, and initial moisture content [21, 22]; type, dosage, and combination of binders and activators [23, 24]; and curing conditions, most notably time and temperature [25, 26].

Yet, despite decades of research, a significant gap remains in the capability to predict the UCS, a critical design parameter, of stabilized soil from its composition and curing time. Most existing predictive models and studies are constrained by a limited number of variables, often focusing on one or two binders and a specific soil type [27, 28]. These studies provide a lot of insight, but their findings cannot be generalized easily. Traditional empirical or statistical models cannot capture or quantify the complex nonlinear interactions within the soil matrix, multiple binders, and chemical activators [29, 30]. Hence, mix design for new projects continues to rely heavily on extensive and expensive trial-and-error laboratory procedures [31].

A holistic approach that can incorporate a wide array of influencing factors, therefore, calls for advancements in the science of soil stabilization and must be data-driven. Large, well-curated datasets open the door for machine learning (ML) and advanced regression techniques to model these complex relationships [32, 33]. Many researchers have begun to explore this path; applications of ANNs, SVMs, and random forests have started to predict a range of geotechnical properties [34, 35]. However, many of the models developed so far are narrow in scope or considered as "black boxes" with no clear interpretation of the governing parameters and thus have limited practical utility to engineers [36-40].

Therefore, the main purpose of this study is to propose a robust, precise, and interpretable predictive model for the UCS of chemically stabilized soils, leveraging a large and diverse experimental dataset. The novelty of the research is that it uses a unique, comprehensive dataset that encompasses a wide range of soil types, a wide variety of binder systems, including conventional and sustainable alternatives, and key chemical activators.

Novelty: Simultaneously providing a generalized prediction for different stabilizing systems, an integrated approach, physical adherence and consistency to already known geochemical behaviors, and predictive uncertainty along with recommendable action for mix design optimization, no prior study has been conducted. The void illustrates a major challenge concerning the practical use of predictive grounded tools in data sustainable ground improvement. The deficiency of engineers' confidence in the system, prediction accuracy and clarity, along with design-oriented outputs, will be addressed.

In this study, the following objectives will be accomplished:

i) The creation of a generalized, highly accurate predictive model for UCS in the varied systems of soil-binder-activator

ii) The predictive uncertainty and reliability, along with the support of geotechnical design to be unencumbered with risk

iii) The dominant physical and chemical parameters for control of strength development; and
iv) The eco-friendly strategies for stabilization

The proposed framework to offer revisions in prediction, sustainable and cost effective stagnation along with details to ease strength development, and its parameters control. This study integrates prediction, interpretation of uncertainty, and optimization, and advances the work tools to enable a paradigm shift in sustainable soil stabilization i.e. designed based stabilization prediction.

2. Data and methodology

This study develops a generalized, physically consistent, interpretable predictive framework on estimating the unconfined compressive strength (UCS) of chemically stabilized soils, while employing a systematic, data-driven approach. The four components of this framework are:

(i) the gathering and statistical characterization of an extensive and varied empirical dataset,
(ii) data preprocessing and preparation of features

(iii) construction and validation of machine learning and/or physics-informed models

(iv) provision of uncertainty and sensitivity analyses.

This systematic approach guarantees predictive validity, generality, and relevance to engineering.

2.1 Dataset Compilation and Statistical Characteristics

Peer-reviewed studies are reviewed in detail, and public databases are surveyed to compile a dataset pertaining to geopolymer and chemically stabilized soils [41]. Initially, an unfiltered dataset consisting of 1485 individual laboratory-tested mixture designs was collected. For quality control purposes, entries that had one or more of the following attributes were removed: Descriptions of the mixture that were vague, missing key variables, or that contained physically impossible values. This resulted in a final dataset consisting of 990 designs to get variation for the model. The final data sample contained a variety of soil-types and a variety of combinations of stabilization systems. The dataset was finally classified into three main categories of the input variables:

1. **Soil physical properties**, including liquid limit, plastic limit, plasticity index, natural water content, and particle size distribution (sand, silt, and clay fractions).

2. **Chemical composition parameters**, expressed in terms of oxide contents (e.g., SiO_2, Al_2O_3, CaO, Fe_2O_3, MgO) representing both soil mineralogy and binder chemistry.

3. **Mix proportions and curing conditions**, including contents of industrial by-products and binders (e.g., GGBS, fly ash, slag, rice husk ash, nano-silica), alkaline activators (NaOH, sodium silicate), water content, and curing time.

The objective variable UCS ranges from 0.01 MPa to 20.47 MPa with an average mean value of 3.16 MPa, recording both marginally and heavily stabilized soils. Such range is significant to help develop models that are able to generalize with varying degrees of stabilization. Figure 1 shows the frequency distribution of the UCS values present in the dataset. As distribution is right-skewed, it demonstrates an increased presence of low to moderately strngth values and a tail end that signifies a greater presence of the most stabilized mixtures. This is a typical distribution for geotechnical strength data and is a demonstration of the variety to be found within the soil–binder systems.

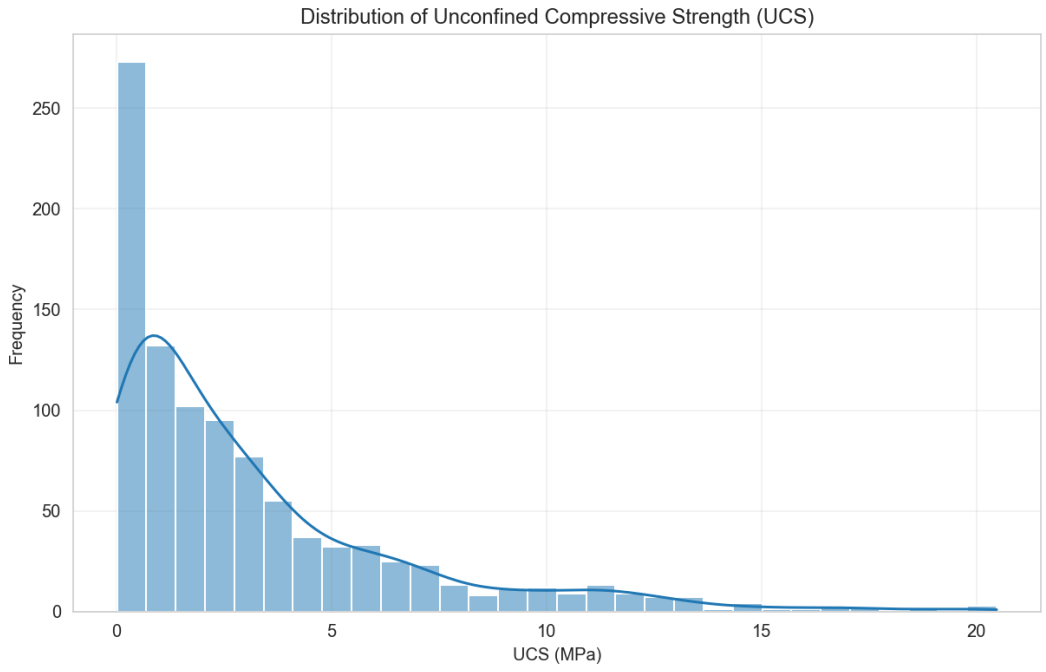

Figure 1. Distribution of UCS values across the compiled dataset

Figure 2 above shows a graph of curing time to illustrate that 28 days is the most frequent curing time, and this is in accordance with laboratory and engineering norms. Data from shorter (less than 7 days) and longer (more than 90 days) curing times is also available to enable modeling of early-age and longer-term strength gains.

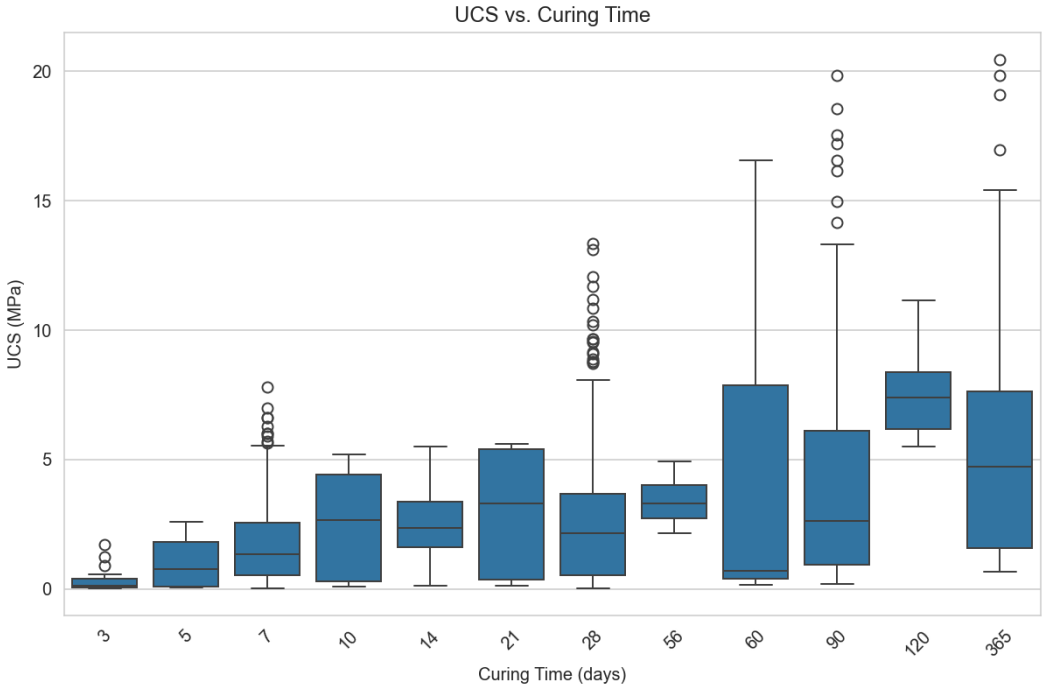

Figure 2. Distribution of curing times for all mixtures in the dataset

The effect of the major mixture components on the UCS is demonstrated using the scatter diagram. Figure 3 illustrates the effect of GGBS content on the UCS. It can be noted that the UCS varies in a positively cumulative manner yet with a wide scattering pattern. Figure 4 illustrates the effect of NaOH content on the UCS. It can be noted that NaOH is a major alkalizing agent in the mixture.

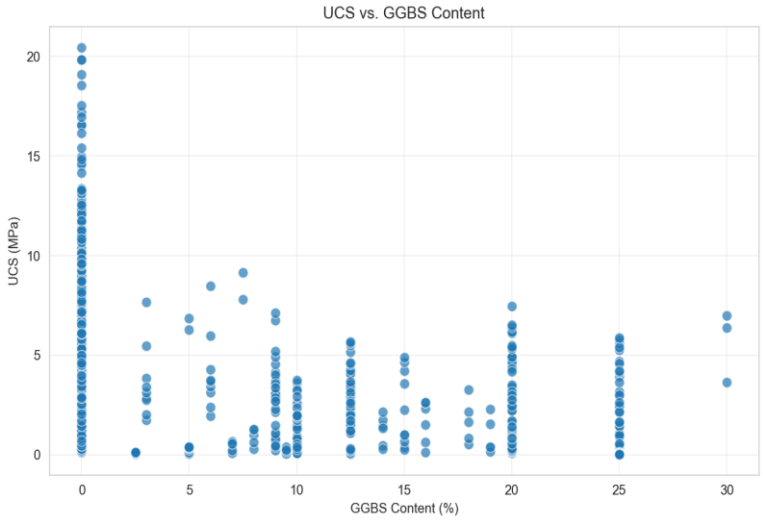

Figure 3. UCS as a function of Ground Granulated Blast-furnace Slag (GGBS) content

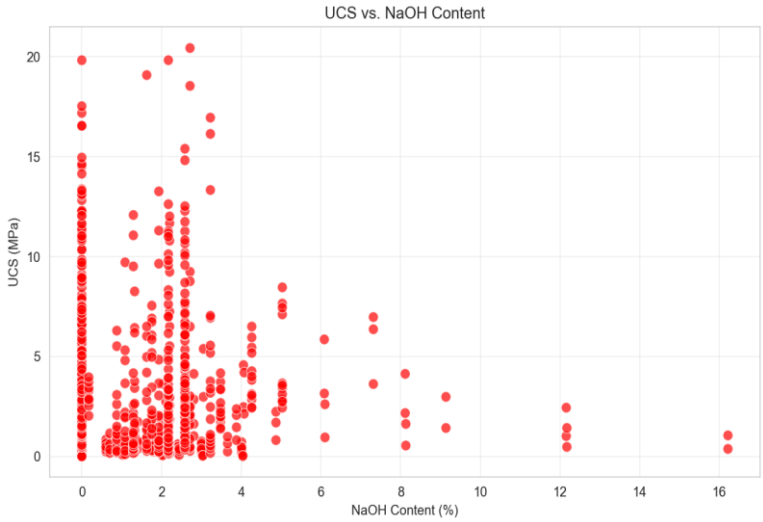

Figure 4. UCS as a function of Sodium Hydroxide (NaOH) content

The Pearson correlation matrix for key input parameters with UCS is represented in Fig. 5. As can be noticed from Fig. 5, curing time and parameters related to binders show positive correlation values for UCS. However, parameters related to water content commonly show negative correlation values. These linear correlations provide preliminary insight but are insufficient to describe the complex nonlinear interactions governing strength development.

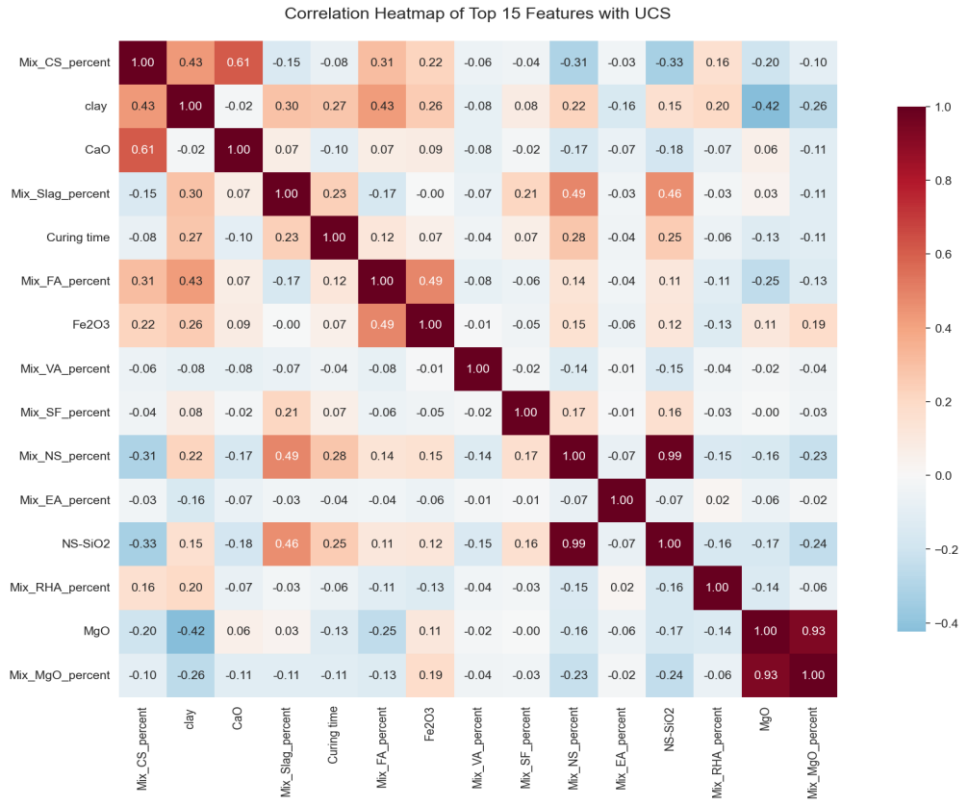

Figure 5. Correlation matrix of key input parameters and the target UCS

Figures 6 and 7 further illustrate the influence of water content and CaO content, respectively. Increasing water content generally leads to reduced UCS due to higher porosity and lower compactness, whereas higher CaO content is associated with increased UCS owing to enhanced formation of cementitious products such as C–S–H and C–A–S–H gels [13,15–17].

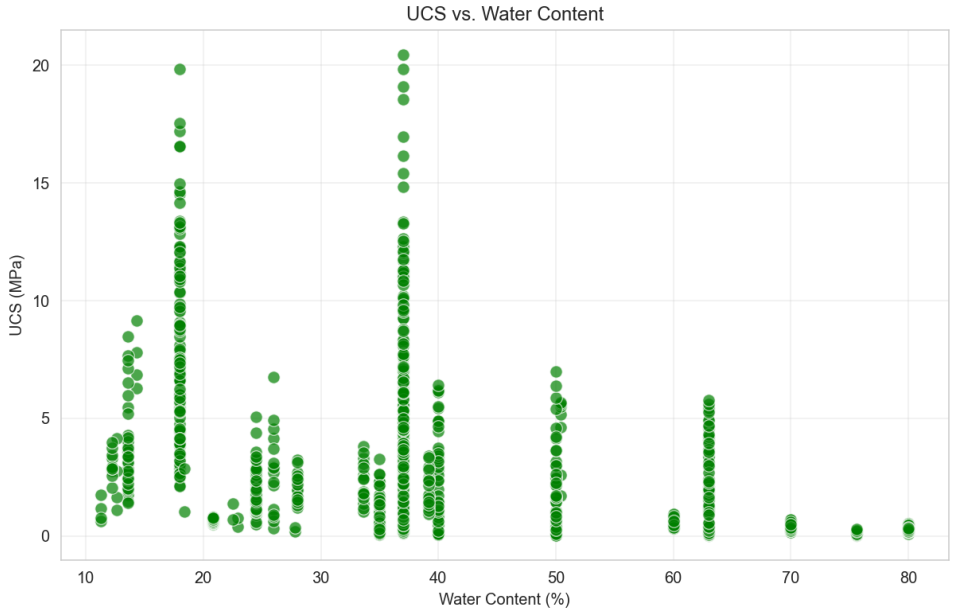

Figure 6. UCS as a function of Water Content

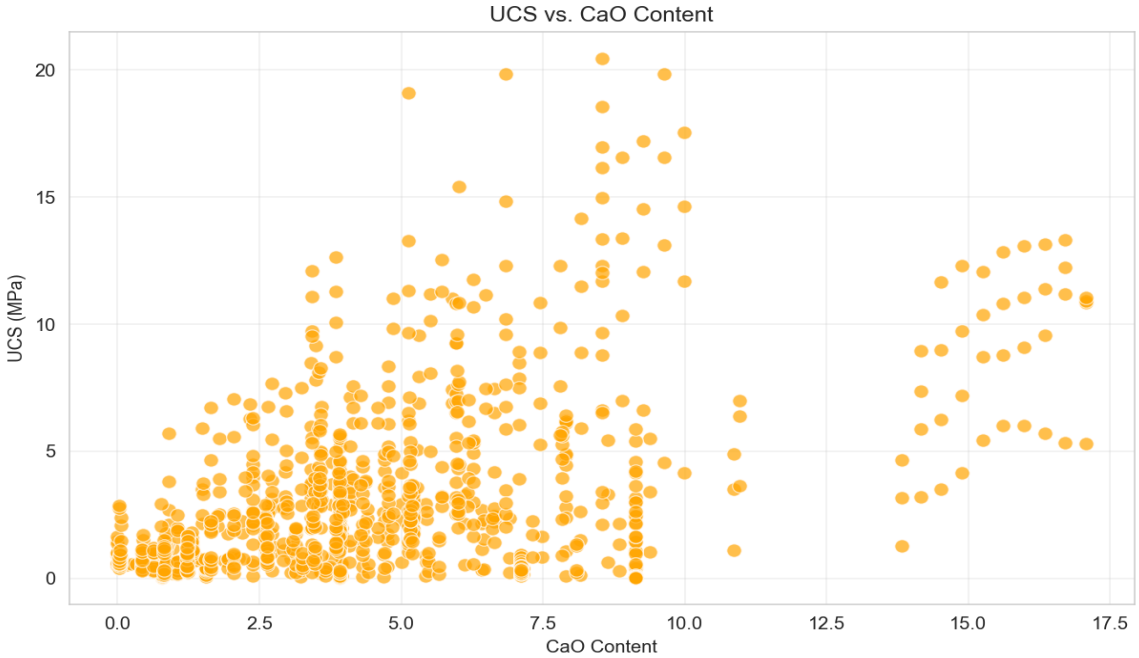

Figure 7. UCS as a function of Calcium Oxide (CaO) content

A scatter plot illustrating how the UCS is influenced by the total CaO content in the mixture, which originates from binders like GGBS, cement, or lime. A positive trend is generally expected, as CaO is a key reactant in the formation of cementitious compounds (C-S-H and C-A-S-H), which are responsible for strength gain.

A statistical summary of the principal variables is provided in Table 1, confirming that the dataset spans a wide and representative range of material properties and mix designs relevant to modern soil stabilization practice.

2.2 Data Preprocessing and Feature Preparation

Prior to model development, the dataset was subjected to preprocessing to ensure numerical stability and unbiased learning. Continuous variables were checked for outliers and physically unrealistic values, which were removed based on engineering judgment and reported experimental bounds. All input features were normalized to a common scale to prevent dominance of variables with larger numerical ranges during model training.

The dataset was randomly divided into training (80%) and testing (20%) subsets, ensuring that the testing data remained completely unseen during model calibration. This split ratio is widely adopted in machine learning applications within geotechnical engineering and provides a balance between model learning and generalization capability [32,33].

2.3. Machine learning modelling framework

To model the highly nonlinear relationship between soil–binder composition and UCS, several machine learning algorithms were implemented and compared. These include linear regression as a baseline model, random forest (RF), extreme gradient boosting (XGBoost), support vector regression (SVR), and artificial neural networks (ANNs). The diversity of algorithms enables benchmarking across linear, tree-based, kernel-based, and deep learning paradigms.

Model performance was evaluated using the coefficient of determination (R^2), mean absolute error (MAE), and root mean square error (RMSE), which are standard metrics for regression problems in geotechnical modeling.

2.3.1 Artificial Neural Network (ANN)

The ANN model was created as a feedforward multilayer perceptron to capture complex nonlinear relationships among input variables. Rectified Linear Unit (ReLU) activation functions were used in the hidden layers to add nonlinearity, while a linear activation function was applied in the output layer. The model was trained with the Adam optimizer by minimizing the mean squared error loss function. The ANN architecture was chosen through repeated adjustments to find the best balance between predictive accuracy and generalization, which helped prevent overfitting.

The mathematical operation of each neuron follows the standard formulation:

$$a_j^{(l)} = g\left(\sum_{k=1}^{m} w_{jk}^{(l)} a_k^{(l-1)} + b_j^{(l)}\right) \quad (1)$$

where $a_j^{(l)}$ is the activation of the j-th neuron in the l-th layer, $g(\cdot)$ is the ReLU activation function defined as $g(Z) = \max(0, z)$, $w_{jk}^{(l)}$ are the weights connecting the k-th neuron in layer $(l-1)$ to the j-th neuron in layer l, $b_j^{(l)}$ is the bias term, and m is the number of neurons in the previous layer.

2.4 Physics-Informed Neural Network (PINN)

In order to improve physical consistency and explainability, a physics-informed neural network (PINN) has been introduced in addition to the conventional ANN. As opposed to the conventional ANN models, the physics-informed ANN has introduced prior knowledge related to geophysical processes in the form of monotonic constraints on loss functions. This helps to

ensure the physical behavior in accordance with existing geochemical principles related to a trend in the increase in UCS values with the increase in curing time and CaO contents, as well as a decrease in UCS values with excess water contents [16, 17,24].

The architecture of PINN includes an input layer with 37 features, three hidden layers with 128-64-32 nodes, and a linear output layer. The role of batch normalization and dropout was to aid in stabilizing training as well as generalization. Even though it was not intended to be more predictive as ANN, it acts as a surrogated interpretational model that can be used for optimization due to its physical correctness.

2.5 Uncertainty Quantification and Sensitivity Analysis

In view of the natural variability of soils and stabilization processes, the uncertainty associated with predictions has been assessed by means of a Monte Carlo simulation method. A total of 10,000 realizations were considered by randomly sampled input variables based on their experimental distribution and by propagating these variables through the developed ANN model.

Sensitivity analyses were conducted to determine which parameters were driving UCS. Feature importance using permutation was first utilized, then SHAP (SHapley Additive exPlanations) to gain global and local interpretations. SHAP values represent how each input feature contributes to its prediction of UCS, providing a direct interpretation between model predictions and physicochemical properties.

Table 1. Statistical summary of the key input variables and target output in the compiled dataset

Variable	Unit	Min	Max	Mean	Std. deviation
UCS	MPa	0.01	20.47	3.16	3.45
Curing time	days	1	365	28*	45.2
GGBS content	%	0	40	12.5	9.8
NaOH content	%	0	8	1.2	1.5
Nano-Silica content	%	0	5	0.5	0.9
Fly Ash content	%	0	35	8.4	7.1
Liquid limit	%	25	85	48.3	15.6
Plasticity index	%	5	55	25.1	11.4

*Indicates the most frequent value (mode).

3. Results and Analysis

This work brings forward the predictive capability analysis of the proposed models, followed by uncertainty analysis and explanation. The results are categorized as:

(i) comparative model assessment

(ii) probabilistic uncertainty analysis

(iii) SHAP analysis, and finally

(iv) physics-informed modeling and optimization.

3.1 Comparative Predictive Performance of Machine Learning Models

The predictive power of the above-developed models: linear regression, random forest regression, XGBoost, SVR, ANN, and MLP models has been evaluated using the independent testing dataset. The above-listed performance metrics have been used for the evaluation of the

predictive power of the above-developed models: coefficient of determination (R^2), root mean square error (RMSE), and mean absolute error (MAE).

Table 2 shows the quantitative performance measures for all models during both training and testing. Among all models, the best generalization ability is found for ANN, followed by XGBoost and SVR models, whereas the worst performance is observed for the linear regression model, which again verifies the nonlinear relationship between UCS and various parameters of soil-binder-curing.

Table 2. Comparative performance metrics of the developed predictive models

Model	R^2 (Train)	R^2 (Test)	MAE (MPa) (Test)	RMSE (MPa) (Test)
Linear regression	0.724	0.712	1.433	2.119
Random forest (RF)	0.978	0.836	0.901	1.597
XGBoost	0.991	0.850	1.047	1.530
Support vector R. (SVR)	0.901	0.867	0.871	1.438
Neural network (ANN)	0.958	0.919	0.674	1.124
Physics-informed ANN	0.901	0.872	0.827	1.410

Figure 8 below demonstrates the parity plot for linear regression between experimental and predicted values of UCS by linear regression models. High variability towards the 1:1 line and a tendency to predict lower UCS levels with increasing UCS values reveal that linear regression models are not effective in representing the nonlinear relationships involved in chemically stabilized soil strength development. **Figure 9** below shows a parity plot of RFR models. Compared to linear regression models, it is evident that RFR has a better distribution of data points close to the 1:1 line for lower UCS levels but has high variability for larger UCS levels.

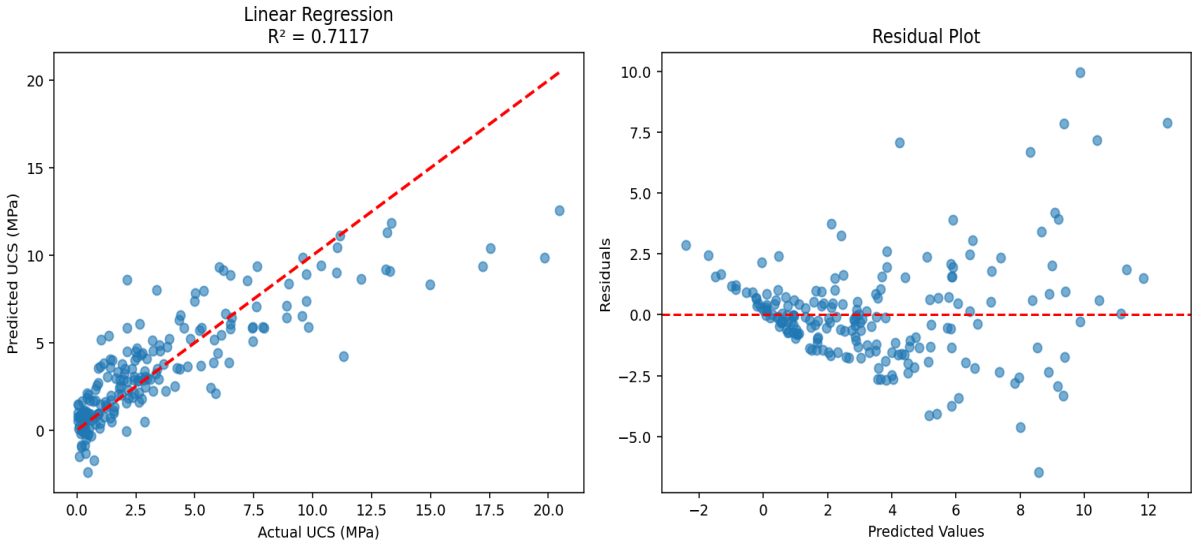

Figure 8. Parity plot: Predicted vs. experimental UCS for the linear regression model

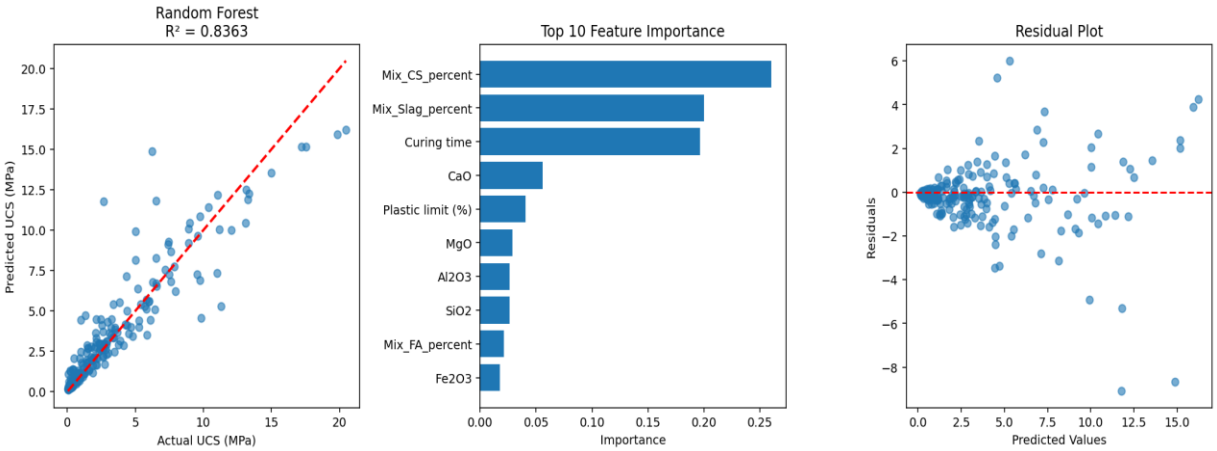

Figure 9. Parity plot: Predicted vs. experimental UCS for the Random Forest model

A parity plot of the XGBoost algorithm is presented in **Figure 10**. This plot suggests a balance of the predicted values about the line of equality that is improved from the RFR algorithm, as a result of the boosting method's effectiveness in eliminating bias. There is, however, a notable scatter of points, particularly at higher UCS values. **Figure 11** shows the Parity plot for the SVR model. The denser distribution of predictions compared to the tree-based models signifies that the kernel model is able to model nonlinear relationships better. Small discrepancies are observed for large values of UCS, which would contain high variability in heavily stabilized mixtures.

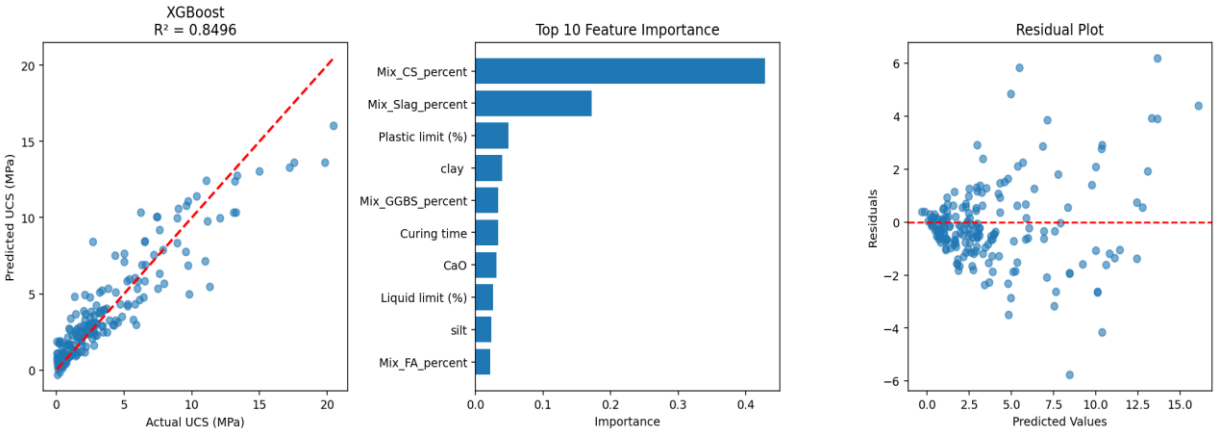

Figure 10. Parity plot: Predicted vs. experimental UCS for the XGBoost model

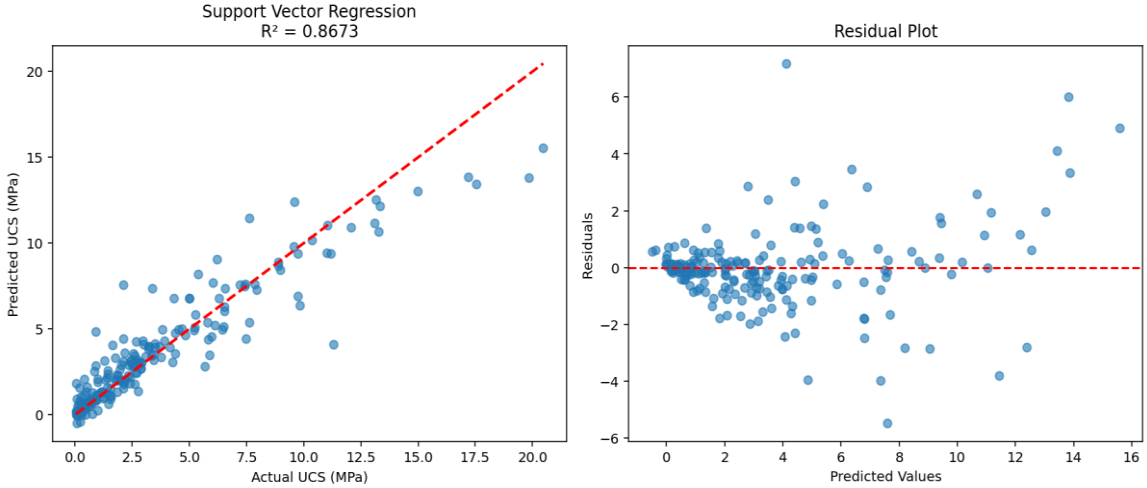

Figure 11. Parity plot: Predicted vs. experimental UCS for the Support Vector Regression (SVR)

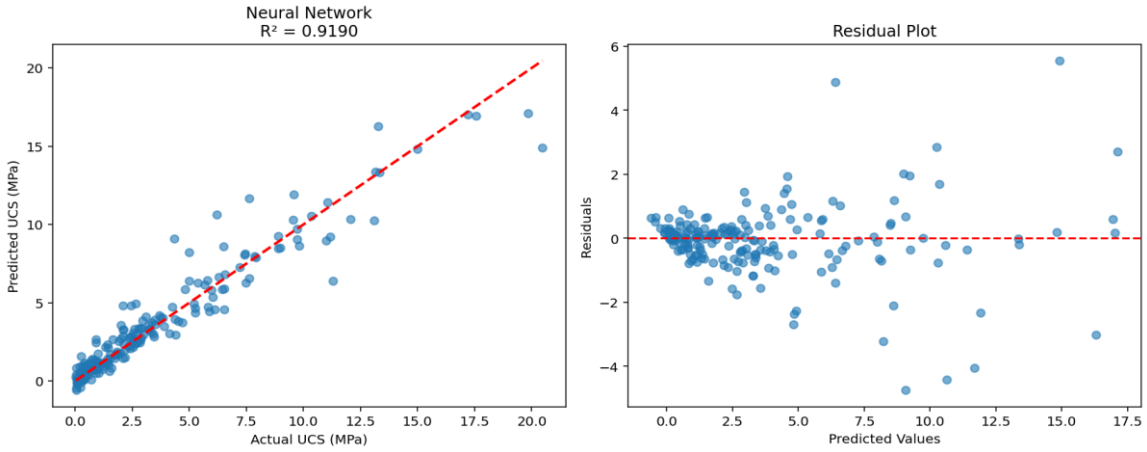

Figure 12. Parity plot: Predicted vs. experimental UCS for the ANN model

Figure 12 presents the parity plot for the ANN model. The tight matching between predicted and experimental data over the entire range of UCS, including high-strength samples, makes it evident that the superior generalization ability of the ANN model enables it to correctly identify

multivariate relationships. Figure 13 presents the parity plot for the MLP model. The MLP model performs satisfactorily to make predictions, whereas its performance is not better than that of the optimized ANN model, emphasizing the significance of modeling architecture that plays an efficient role in deep learning-based geotechnical models.

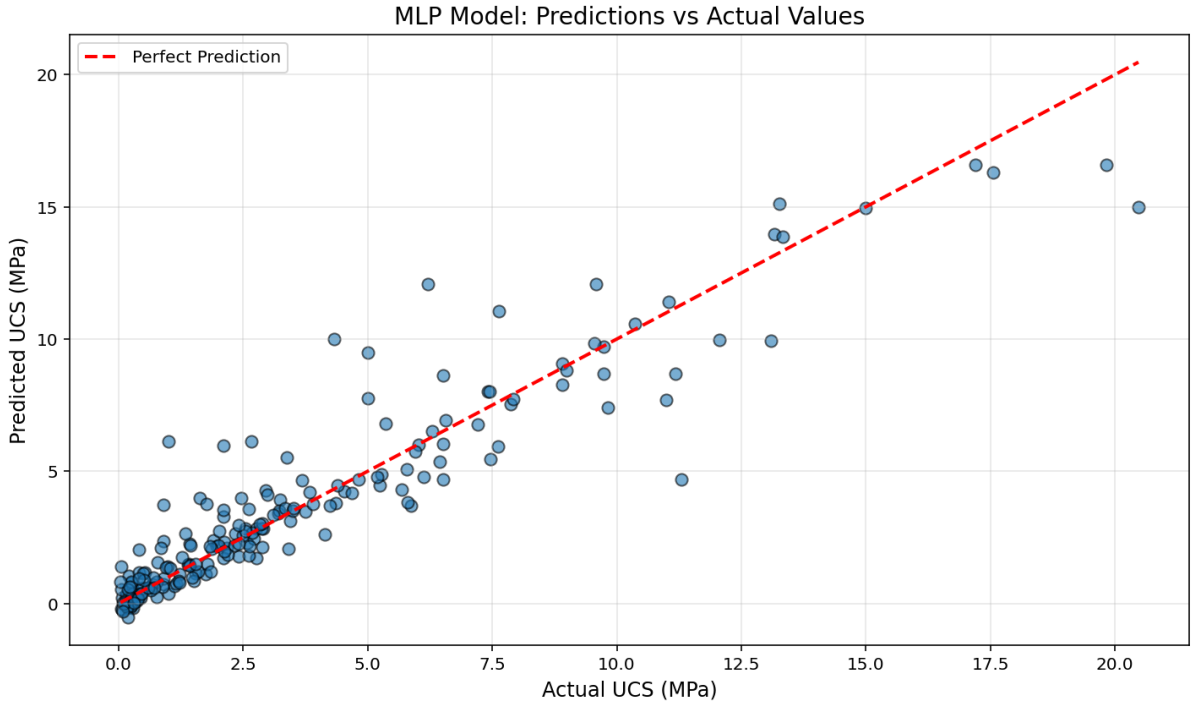

Figure 13. Parity plot: Predicted vs. experimental UCS for the MLP model ($R^2 = 0.872$).

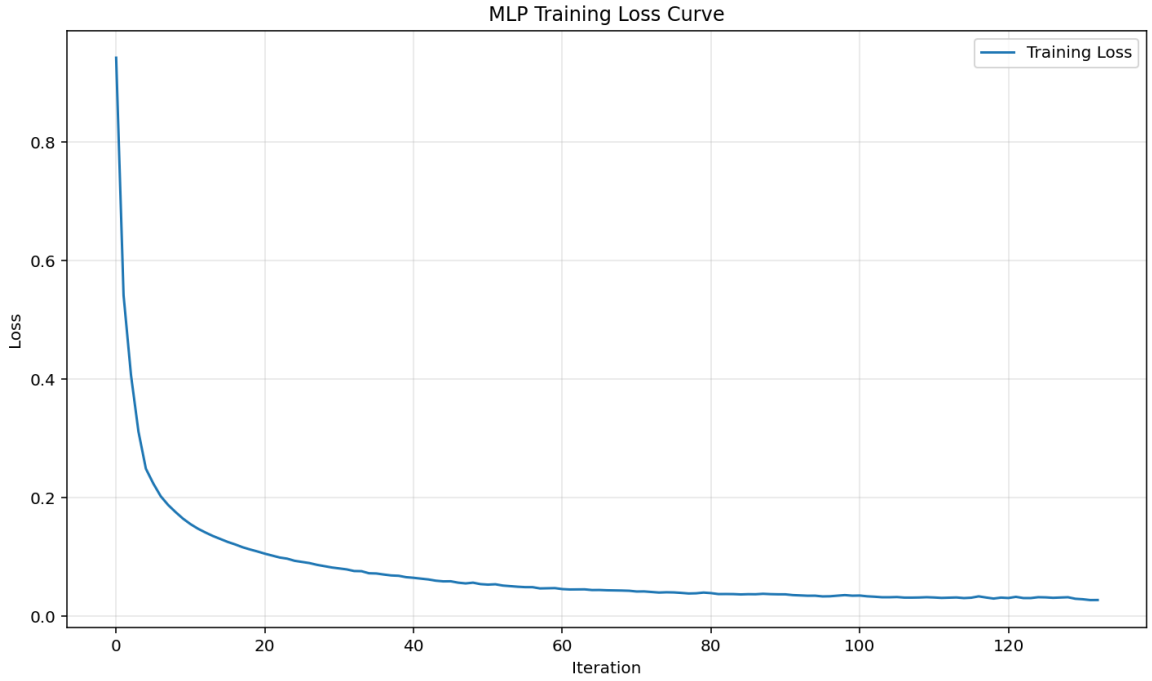

Figure 14. Training and validation loss curves for the MLP model across epochs

Figure 14 illustrates the training and validation loss curves for MLP. The smooth convergence curve and slight differences in the training and validation loss values show that MLP is having a stable training process without any signs of overfitting.

3.2 Uncertainty Quantification Using Monte Carlo Simulation

To account for natural variability associated with soil properties as well as reaction of soil stabilization, uncertainty analysis was performed by using a Monte Carlo simulation with 10,000 realizations based on the developed ANN model. Table 3 lists the statistical descriptors of the predicted distribution of the UCS, mean values, standard deviations, and confidence intervals. The distribution of the predicted UCS values was summarized in Table 3, while Figure 15. illustrates the distribution.

Table 3. Statistical summary of the predicted UCS from the Monte Carlo simulation.

Statistic	Value
Mean predicted UCS (MPa)	2.64
Standard deviation (MPa)	1.47
Coefficient of variation (%)	55.7
5th percentile (MPa)	0.52
95th percentile (MPa)	5.14
95% confidence interval (MPa)	[0.52, 5.14]

Figure 15 presents the probability density function (PDF) of UCS obtained from Monte Carlo simulation. The right-skewed distribution reflects the combined influence of material heterogeneity and nonlinear chemical reactions. **Figure 16** shows the cumulative distribution function (CDF) of UCS, enabling direct extraction of reliability-based UCS thresholds for design purposes.

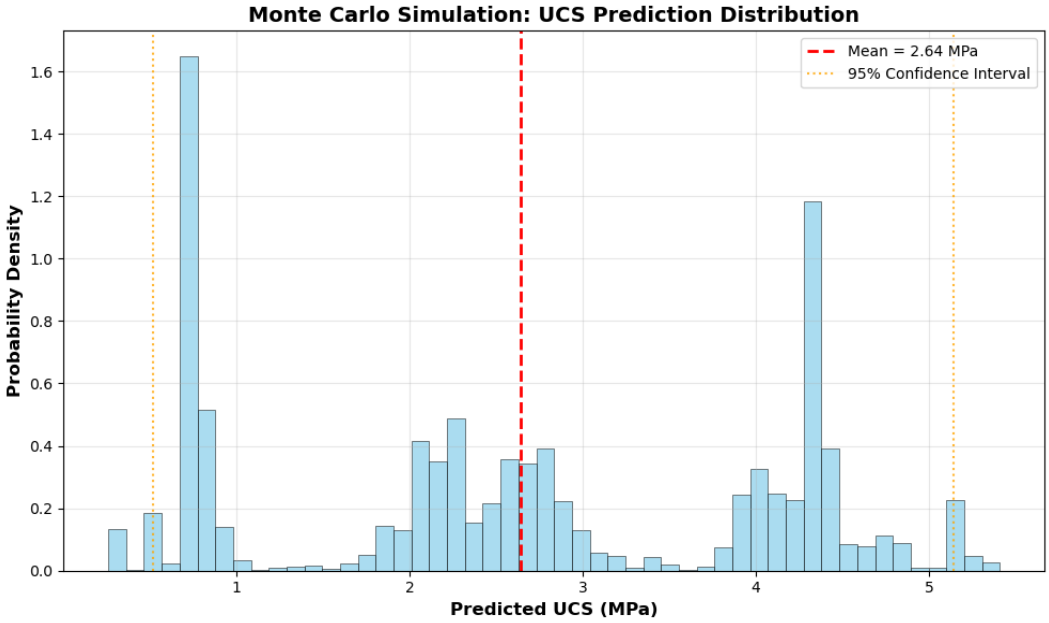

Figure 15. Probability density function of predicted UCS from the Monte Carlo simulation

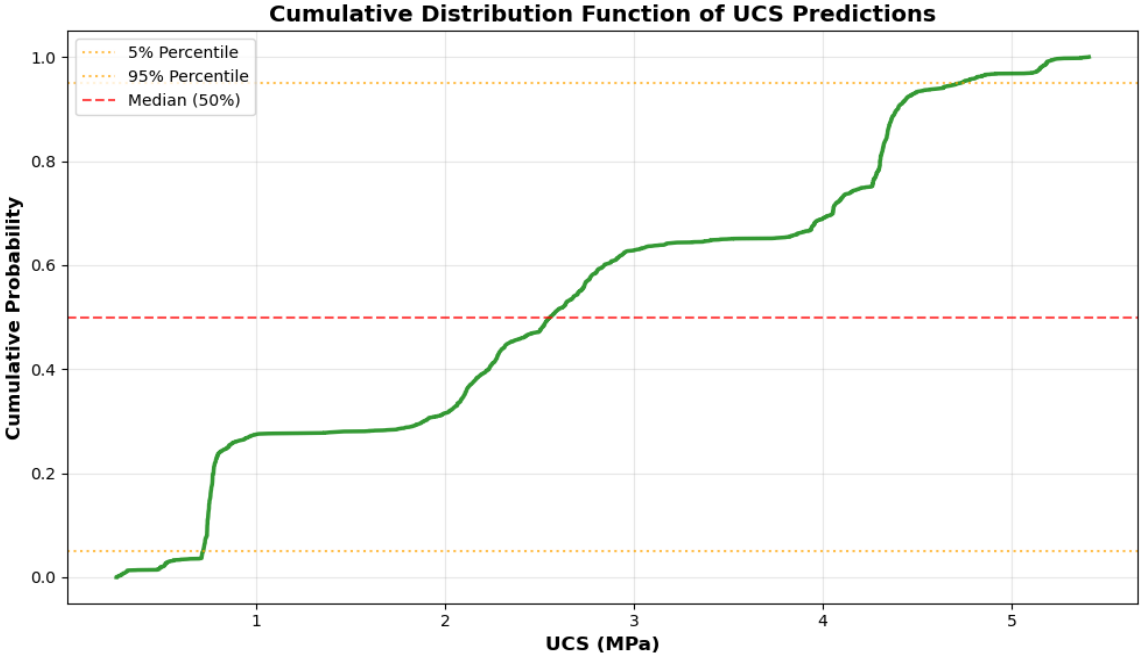

Figure 16. CDF of predicted UCS

Figure 17 presents the exceedance probability curve, illustrating the likelihood that UCS exceeds specified strength levels, which is directly relevant for performance-based geotechnical design.

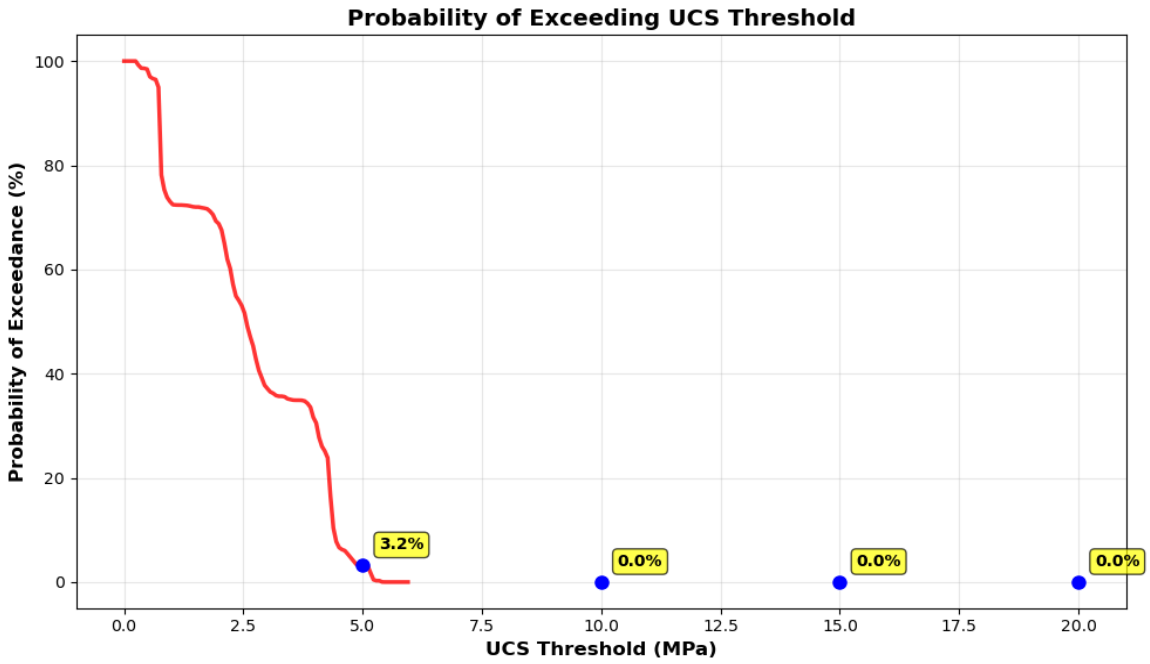

Figure 17. Exceedance probability of predicted UCS

Figure 18 compares the experimental UCS distribution with Monte Carlo–predicted results, demonstrating good agreement in both central tendency and dispersion. Figure 19 presents a box-plot comparison of experimental and predicted UCS values, further confirming that the model reproduces the variability inherent in laboratory data. Figure 20 illustrates the convergence of Monte Carlo simulation results, showing stabilization of mean and standard deviation well before 10,000 iterations.

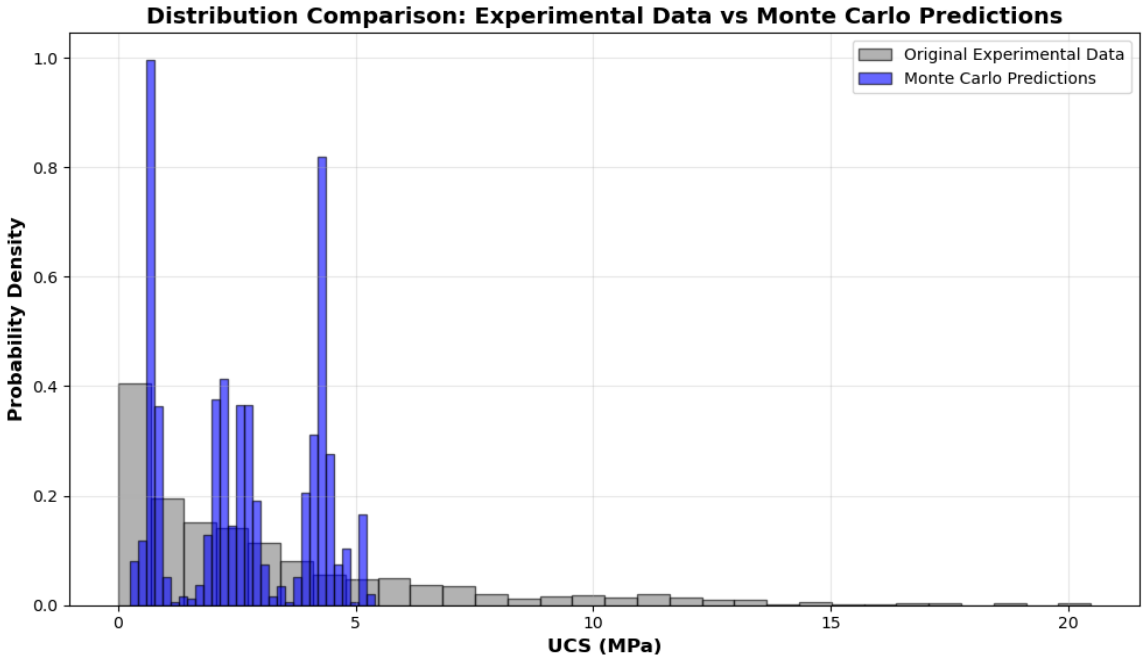

Figure 18. Direct comparison of the original experimental UCS distribution and the Monte Carlo predicted distribution

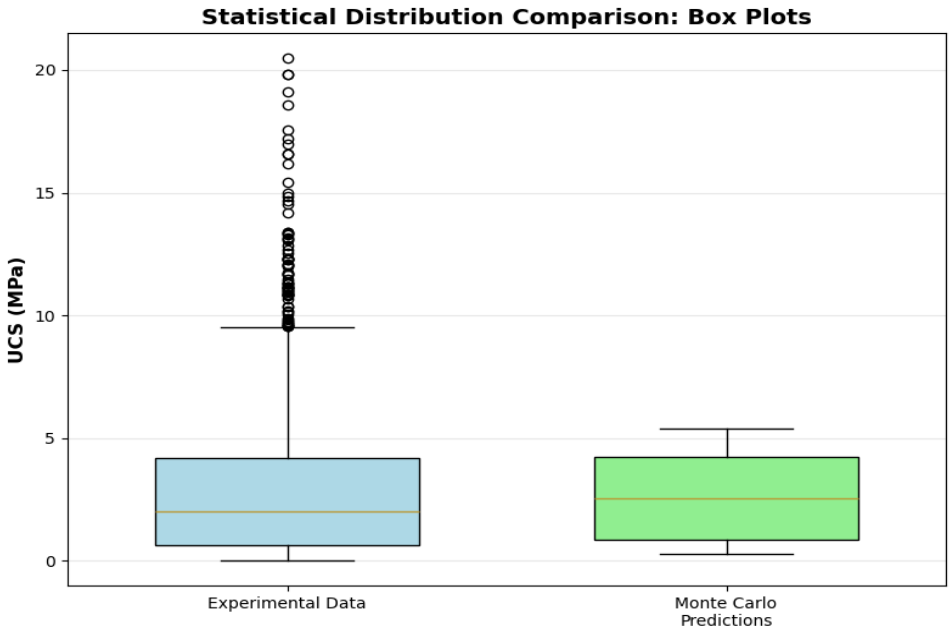

Figure 19. Box plot comparison of the original experimental data and the Monte Carlo predictions

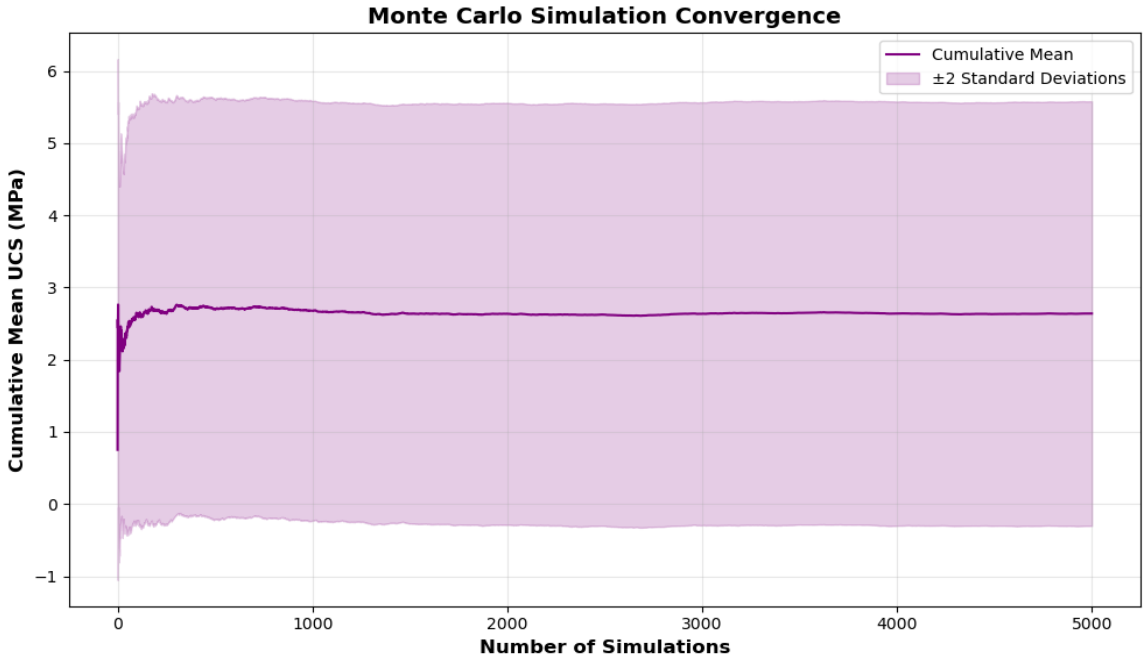

Figure 20. Convergence of the Monte Carlo simulation for the mean and standard deviation of predicted UCS

3.3 SHAP-Based Interpretability and Governing Parameters

To interpret the ANN predictions and identify the dominant parameters influencing UCS, SHAP analysis was employed.

Figure 21 presents the SHAP summary plot ranking input variables by their global importance. Curing time emerges as the most influential parameter, followed by binder content and alkaline activators, while water content shows a predominantly negative contribution.

To further explore the nature and direction of influence of the most critical parameters identified through SHAP analysis, dependence plots for the top three features curing time, water content, and CaO were examined (Figure 22). These plots depict the relationship between the actual feature value (x-axis) and its corresponding SHAP value (y-axis), with points colored by the value of the most interacting secondary feature.

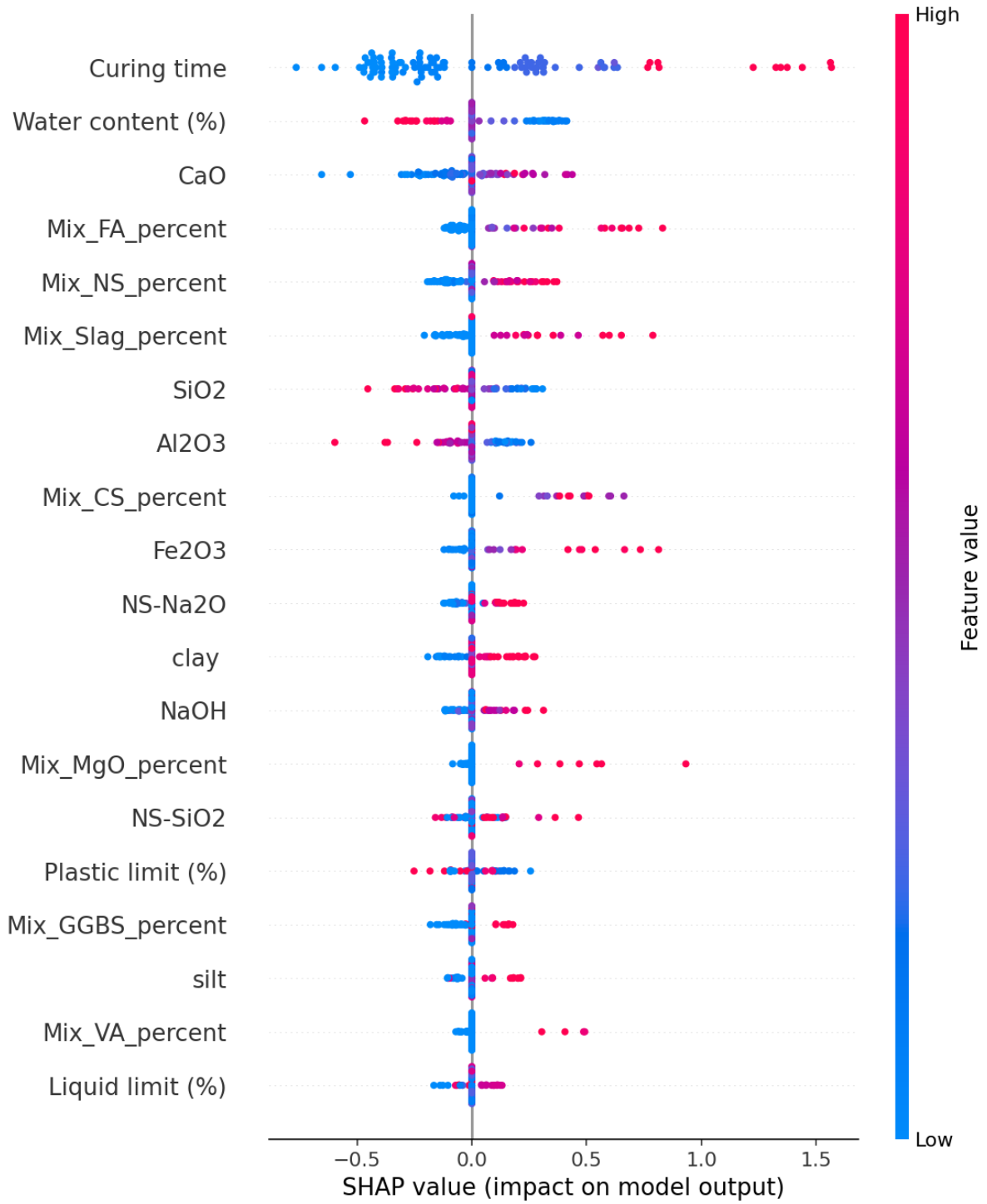

Figure 21. Global sensitivity analysis: SHAP summary plot (violin distribution) for the ANN model inputs

Curing time (Figure 22a) indicates a strong positive monotonic relationship where the longer the curing time, the larger the SHAP values corresponding to higher UCS. Significantly, the CaO composition-based coloring indicates a crucial interaction where high CaO-containing

samples are generally found in the upper-right corner, translating that the longer curing time benefit is further accentuated in high CaO-containing systems. Notably, the well-documented interaction between longer curing time and high CaO availability has long been recognized as a critical parameter facilitating the development of cementitious C-S-H/C-A-S-H gels [16, 17].

Water content (Figure 22b) shows a mainly negative relationship with SHAP values, further supporting that high values of moisture content are usually associated with lower UCS predictions. It is worth noting that the spread of points widens within the range of medium levels of water content (15%–25%), where it can be noticed that due to color representation based on curing time, longer curing times can counteract the negative impact of high water content on concrete strength.

CaO (Figure 22c) shows a positive saturating relationship, where the SHAP values show a steep rise up to a certain point of around 10–12% CaO beyond which the addition of CaO shows diminishing returns. The graph is colored in accordance with the SiO2 composition, thereby indicating that the systems with higher availability of SiO2 (red dots) show higher values of SHAP corresponding to a certain composition of CaO, thus highlighting the importance of optimal CaO/SiO2 ratios [13, 15].

These dependence graphs go beyond simple feature ranking and highlight the complex, non-linear relationships that determine the process of UCS evolution. These graphs offer valuable recommendations for the optimization of component proportions, such as the cumulative influence of the curing time and CaO, or the relationship between the content of water and the curing time.

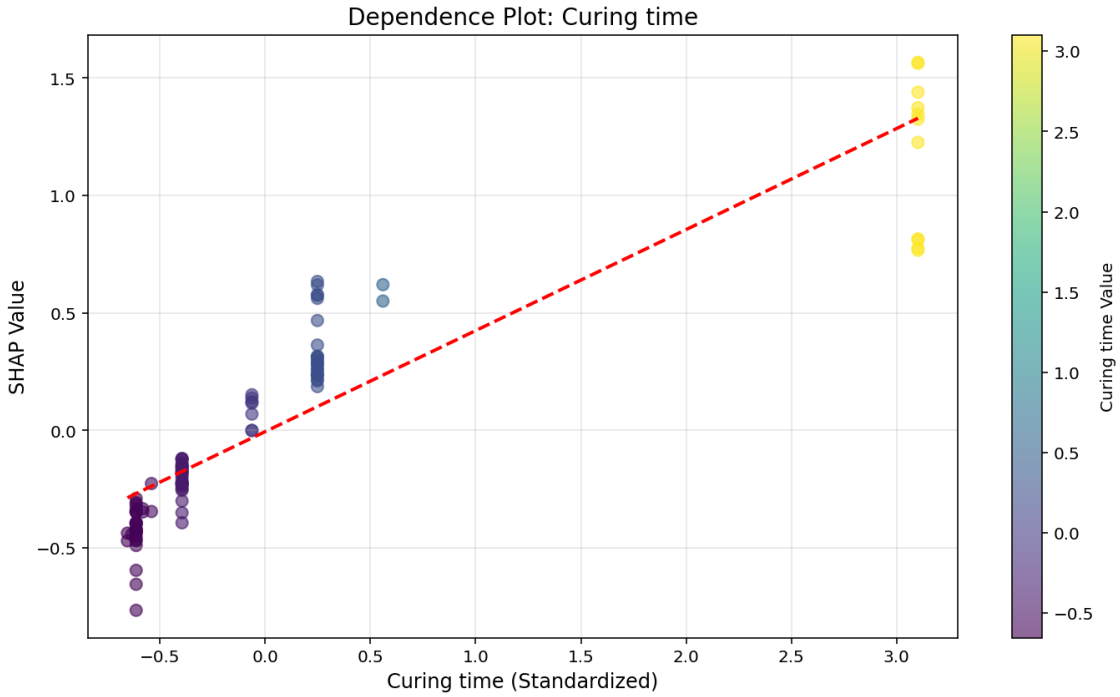

Figure 22 (a)

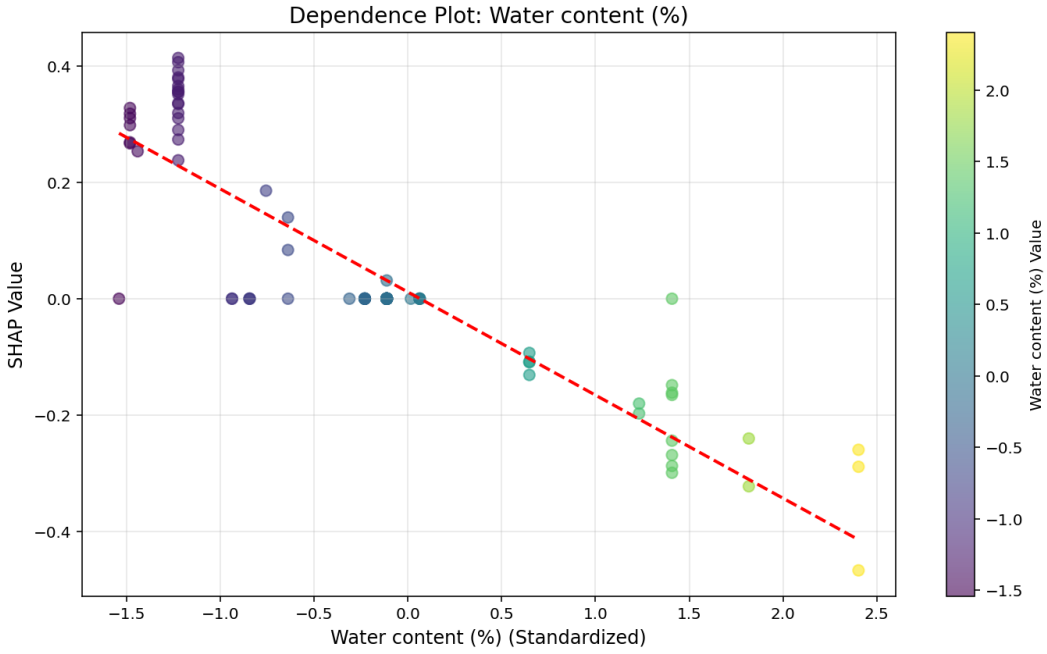

Figure 22 (b)

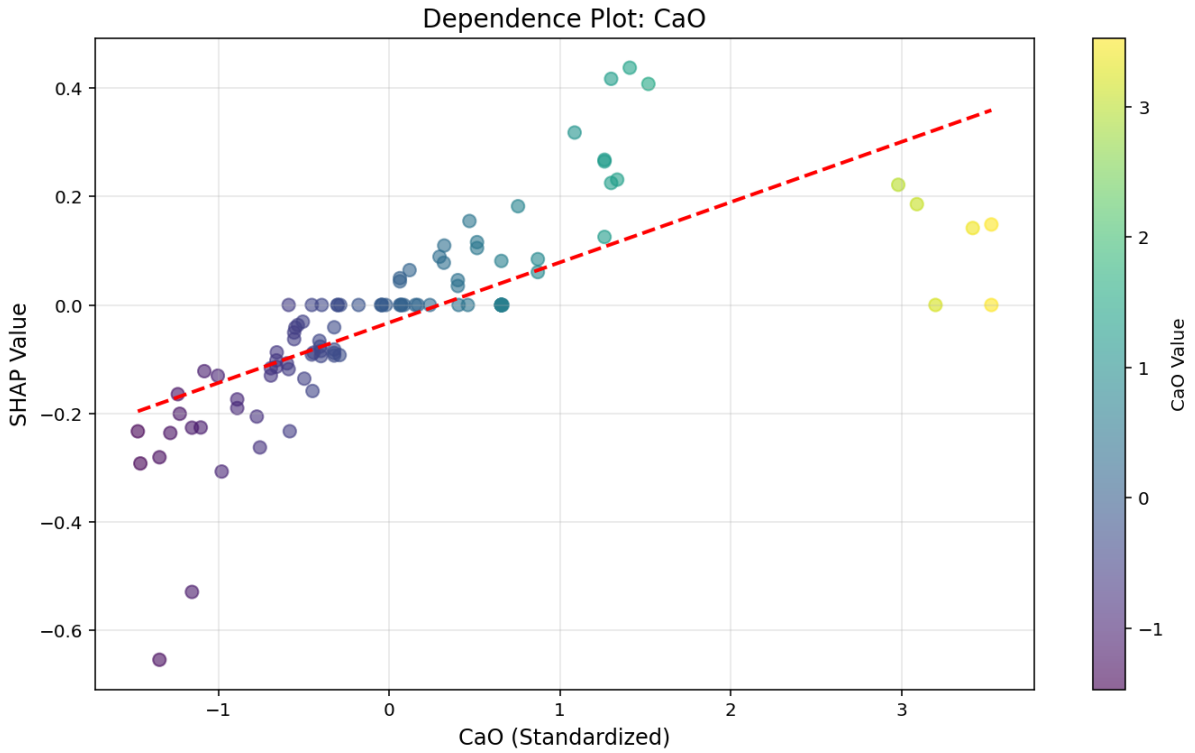

Figure 22 (c)

Fig. 22. SHAP dependence plots for the top three influential features: (a) curing time, (b) water content (%), and (c) CaO content

Finally, the associated reliability analysis in Figure 23 above further confirms the reliability of the model performance; given the high probability of 80% that the well expectancy value of the test error would not exceed 1.5 MPa. Based on the high reliability of the performance requirements, the interpretability of the model is a useful tool in the optimization of the mix design process, the minimization of laboratory test mixes, and the effective utilization of industrial by-products with immense value. The graph above illustrates the cumulative probability of the absolute error of the predictions, which means there is an 80% chance that the absolute error will be below 1.5MPa.

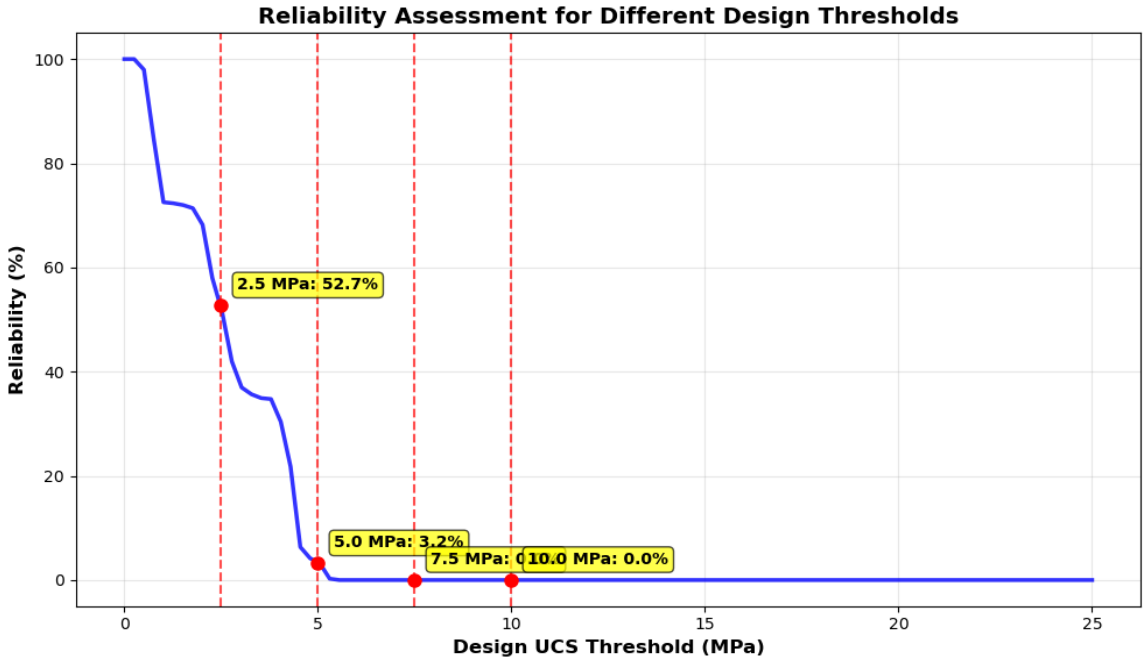

Figure 23. Reliability assessment: Cumulative probability of the absolute prediction error

Importantly, the SHAP-based interpretations presented herein are not intended as purely statistical explanations, but rather as data-driven confirmations of well-established geotechnical and geochemical mechanisms governing strength development in chemically stabilized soils.

3.4. Physics-informed neural network with SHAP interpretability and multi-objective optimization

To further develop the predictive framework with the goal of reaching physically consistent, interpretable, and optimization-ready models, a Physics-Informed Neural Network (PINN) has been developed, further incorporating SHAP explanatory methods and multi-objective optimization techniques. The integrated framework promotes a hybrid paradigm, bridging the gap from data-driven prediction to the inclusion of domain knowledge for interpretation and automated mix design optimization.

3.4.1. PINN architecture and training

The PINN consisted of a feed-forward neural network with three hidden layers (128-64-32 units) with batch normalization and dropout probability (p = 0.1). The input layer received the 37 variables, and the output layer was a single UCS prediction. The most unique aspect is the loss function, written as the sum of a data fidelity term, using the mean squared error between predictions and experimental UCS, and a physics-based regularization term that captures the expected monotonically increasing dependence on curing time and CaO, and monotonically decreasing dependence on excess water, and so on, for UCS, as expected by basic geochemical principles [16, 17, 24].

In chemically stabilized soils, a monotonic increase of UCS with curing time and related factors of binders should be anticipated under otherwise equal conditions. To enforce this physically consistent behavior, a physics-based penalty term was incorporated into the ANN loss function.

$$\mathcal{L}_{Total} = \mathcal{L}_{data} + \lambda_p \mathcal{L}_{physics}$$

Where

$$\mathcal{L}_{data} = \frac{1}{N}\sum_{i=1}^{N}(UCS_i^{pred} - UCS_i^{exp})^2$$

and the physics-based penalty term is defined as:

$$\mathcal{L}_{physics} = \frac{1}{N}\sum_{i=1}^{N} \max(0, -\frac{\partial UCS^{pred}}{\partial t_c})$$

Here, t_c denotes curing time. The penalty term will be active only when the predicted UCS does not follow the monotonic trend expected in the physical behavior (i.e., the gradient turns negative). The weight coefficient λ_p balances the priority given to consistency and data representation and was set after cross-validation experiments. The training process for the model involved 150 epochs using the Adam optimizer, and the training and validation loss are represented in Fig. 24. That the training and validation loss converged to similar values (final loss of 1.66 and 1.46, respectively) and no significant gap is observed between them confirms the learning process accurately and efficiently without any possibility of overfitting. The results obtained by the PINN, in terms of test accuracy of RMSE = 1.2075 MPa and $R^2 = 0.881$, are not as accurate as the ANN results, but they are far better in terms of consistency and understanding of the underlying phenomenon.

It is reinforced here that the physics-informed neural network is not designed for the purpose of statistically outperforming the optimized ANN in the context of standard accuracy metrics like R^2 and/or RMSE. Instead, the primary value of the PINN lies in enhancing extrapolation safety and physical consistency by enforcing monotonic and physically admissible trends in UCS evolution, particularly under sparsely sampled or uncertain regions of the input space.

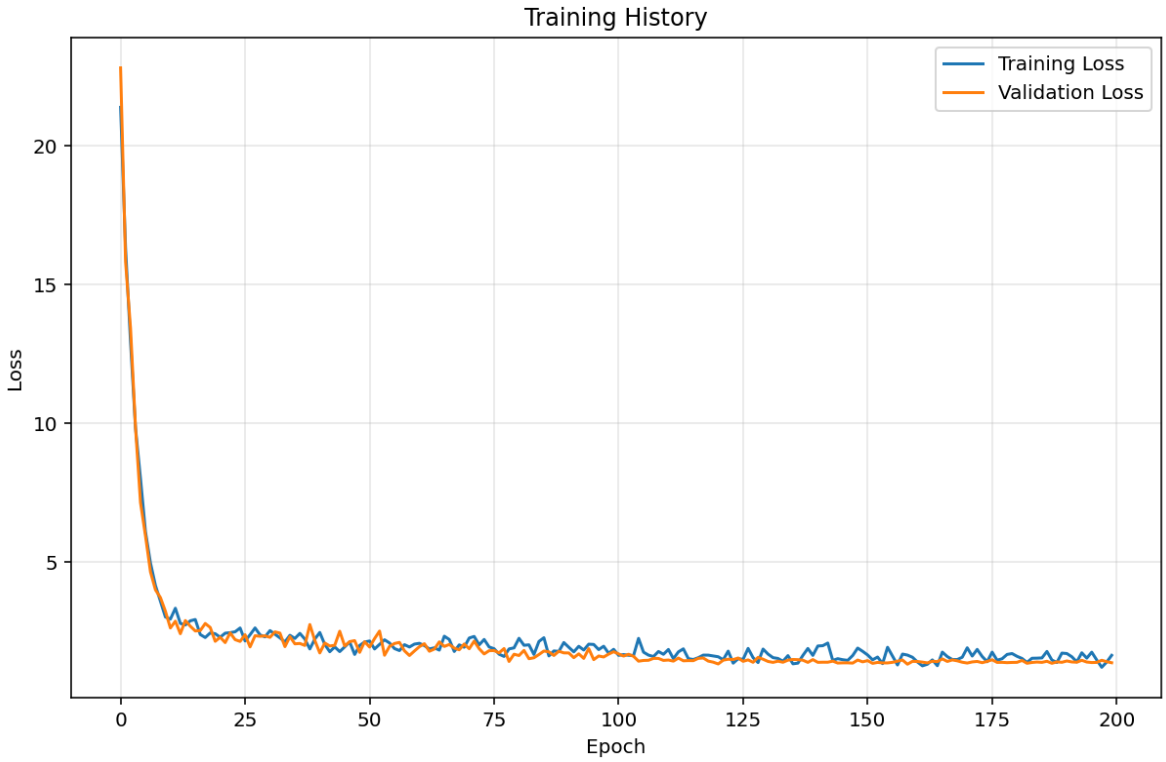

Figure 24. Training and validation loss curves for the Physics-Informed Neural Network (PINN) over 150 epochs

Beyond enforcing monotonic trends, the incorporation of physics-informed constraints reduces the likelihood of physically implausible UCS predictions under extrapolative and uncertain input conditions, which are commonly encountered in field-scale soil stabilization practice.

3.4.2. SHAP-based interpretability of the PINN

A SHAP analysis of the trained PINN helped in understanding how the physical constraints made a difference in terms of feature importances. The results obtained in the form of a summary plot (Fig. 25) discuss how curing time is still playing the most crucial role in this respect, CaO content, and water content. Interestingly enough, this time the PINN is stressing more on CaO and SiO_2, which are primary reactants in the preparation of the cementitious gel.

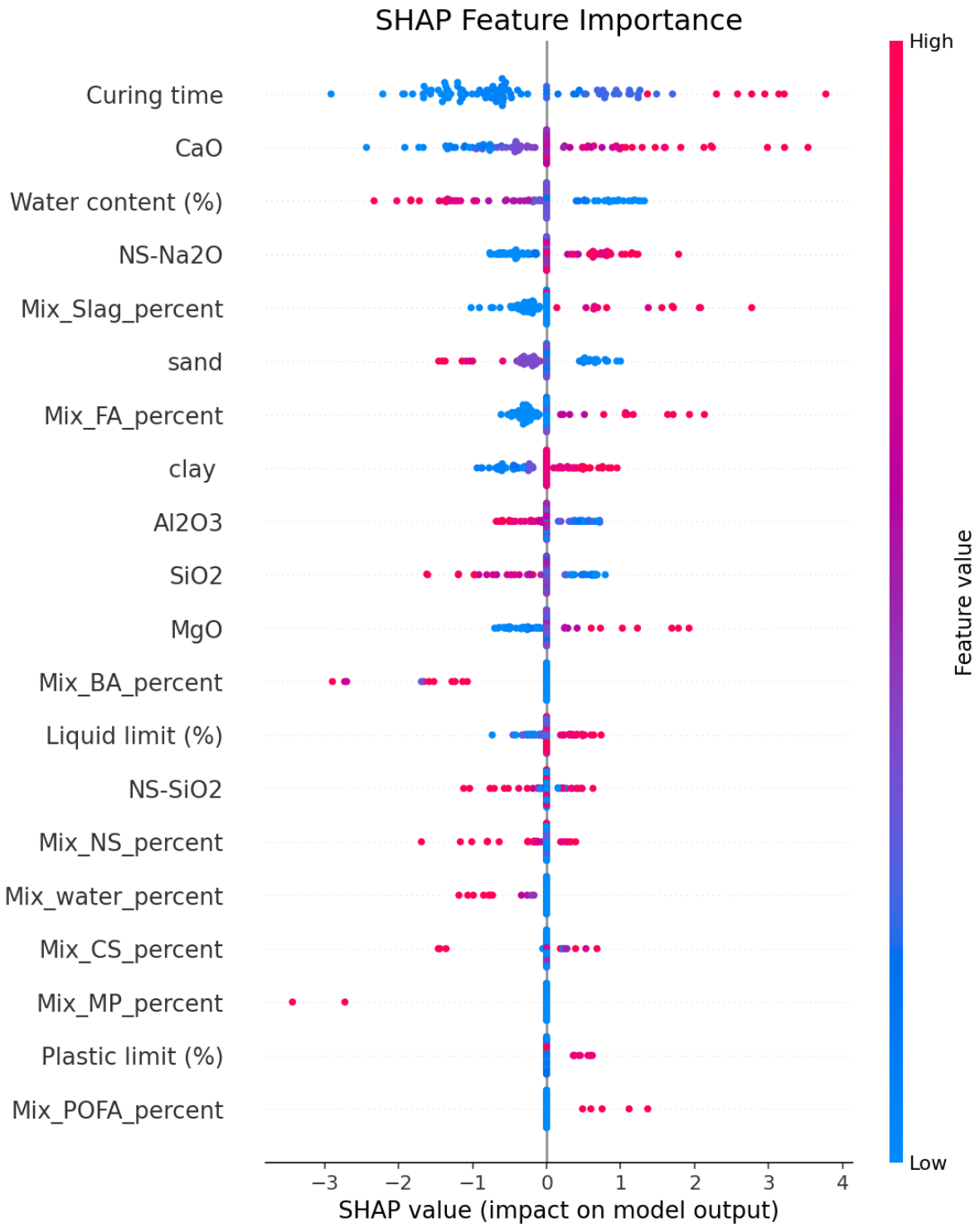

Figure 25. SHAP summary plot for the PINN model, showing feature importance distributions

3.4.3. Multi-objective optimization for sustainable mix design

Utilizing the trained PINN as a surrogate model, a multi-objective optimization problem was solved to obtain Pareto-optimal mix designs aiming to the simultaneous optimization of UCS and material minimization.

To allow the mix design for optimization purposes, a simplified cost approach was developed using material ratios generally employed in chemical soil stabilization.

Linear cost function

$$c = \sum_{j=1}^{M} c_j x_j$$

where:

- C = total material cost per unit volume of treated soil
- x_j = proportion (or dosage) of the j^{th} material
- c_j = unit cost of the j^{th} material

Materials include binders (e.g., GGBS, fly ash), alkaline activators, nano-additives, and water.

Multi-objective optimization formulation

$$Maximize\ UCS\ (x_1, x_2, \ldots., x_M)$$

$$Minimize\ C(x_1, x_2, \ldots, x_M)$$

subject to:

$$x_j^{min} \leq x_j \leq x_j^{max}$$

The resulting optimization problem was solved with a Pareto-based multi-objective formulation, and a set of Pareto optimal solutions has been found. This set represents a set of trade-offs between maximizing concrete strength and minimizing material costs. Formulation of the above-mentioned optimization problem enables designers to define mix designs that satisfy certain constraints.

A differential evolution algorithm has been used to obtain the Pareto-front (Figure 26) where the trade-off between strength and economy takes place. From the Pareto set, an optimum solution has been taken, aiming for a predicted ultimate compressive strength of 15.2 MPa, with less consumption of the high-cost activators nano-silica and NaOH. Mix proportion wise, more GGBS and fly ash content, low-carbon-footprint industrial by-product, sustainable, cost-effective stabilization techniques are being described.

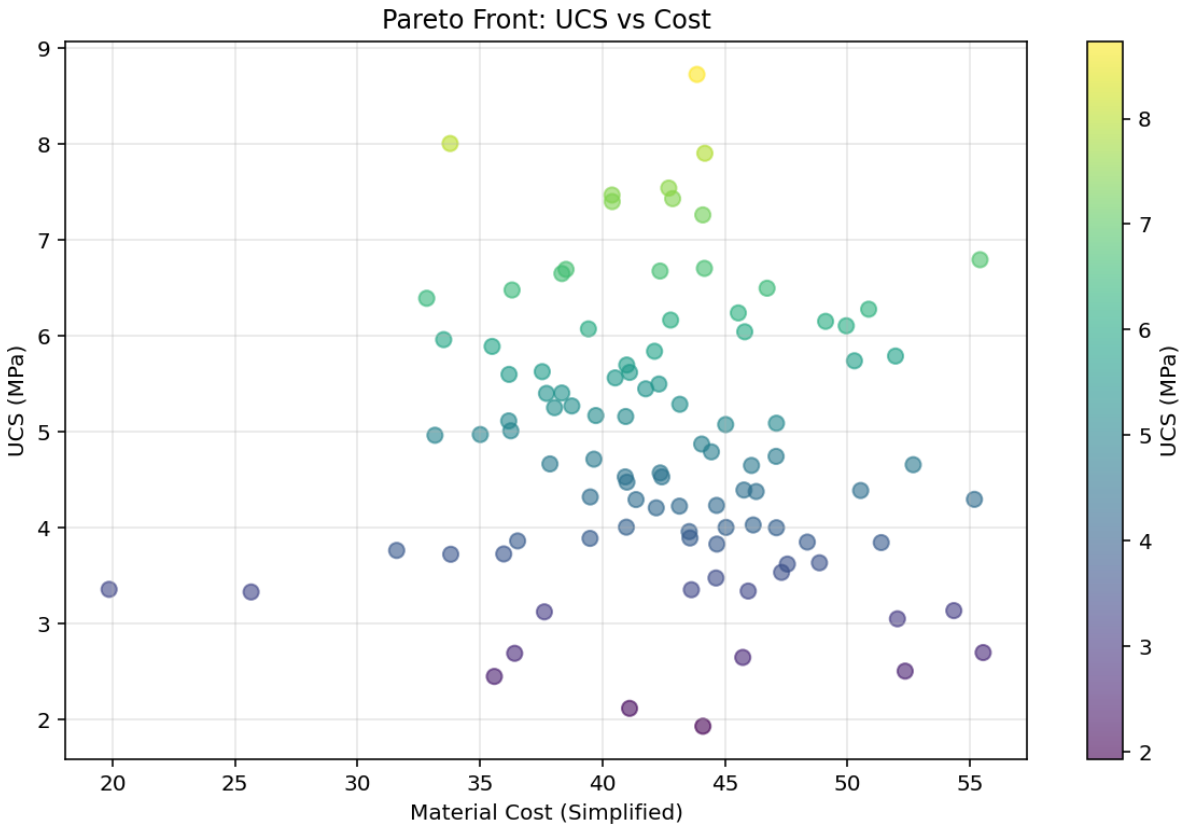

Figure 26. Pareto front from multi-objective optimization using the PINN surrogate model

Table 5. Characteristics of three representative optimal solutions extracted from different regions of the Pareto front

Parameter	Solution A (Cost-optimal)	Solution B (Balanced)	Solution C (Performance-optimal)
Predicted UCS (MPa)	5.2	9.8	15.2
Estimated Cost ($/m³)	28	45	78
GGBS (%)	18	18	24
Fly Ash (%)	14	12	10

Parameter	Solution A (Cost-optimal)	Solution B (Balanced)	Solution C (Performance-optimal)
Nano-silica (%)	0.0	1.2	2.1
NaOH (M)	0.8	1.8	3.2
Water Content (%)	16.2	15.8	14.5
Curing Time (days)	28	42	90
Key Application	Low-traffic pavements	General subgrade	Critical infrastructure

Table 5 shows properties of three illustrative optimal solutions obtained from varying locations on the Pareto fronts depicted in Fig. 26. These solutions illustrate the performance-cost compromise obtained by the multi-objective optimization approach, providing a focused set of designed mixes for given engineering applications. Solution A corresponds to the cost-efficient region, Solution B corresponds to the 'knee point solution' around the region where marginal increase in costs result in significant improvement in strength, and Solution C corresponds to the performance-efficient region, documenting maximum potential strength regardless of the material normalization aspect. The values for the parameters were obtained from the differential evolution optimization process and are true representation points on the Pareto fronts, always proven to stick to the feasible region as established by the experimental study [41]. Cost estimates were established based on regional average construction material prices for the industry (2023-2024), indexing by-products such as GGBS and Fly Ash with relatively low-cost coefficients given the waste material origin [11, 15]. The final column, 'Key

Application', helps engineer the selection and adoption of designed mixes depending on the engineering applications and limitations, resulting in devising interpretative engineering solutions for the optimization process outcome.

Results from Sections 3.1 to 3.4 below present an integrated and sequential framework of analyses rather than being independent of each other. The comparison in Section 3.1 identifies the optimized ANN as the best data-driven predictor of UCS, which then forms the baseline model for uncertainty propagation in Section 3.2. Monte Carlo simulations quantify explicitly the dispersion in ANN predictions due to variability in input parameters, converting a point prediction into probabilistic design information. Mechanistic insight into these uncertainties is then provided by SHAP-based interpretability analysis in Section 3.3, identifying curing time, binder content, and water content as the dominant contributors that control both the magnitude of the prediction and the variability thereof. These SHAP-derived trends directly inform the feasible bounds and priority variables used in the multi-objective optimization of Section 3.4, ensuring that optimization is guided by parameters that are physically meaningful and statistically influential. Finally, the incorporation of physics-informed constraints within the PINN framework enhances the robustness of predictions under extrapolative and uncertain conditions by enforcing monotonic strength evolution, thereby complementing the data-driven ANN with physically consistent behavior across the explored design space.

4. Conclusion

The proposed research presents a reliable data-driven approach that has effectively been established for the estimate of the UCS value for chemically stabilized soils. This responds to the solutions found for what is arguably the most urgent issue associated with reliable geotechnical engineering practices. With a detailed collection of 990 laboratory mixes, ranging

from varying soils and industrial materials, as well as varying chemical activators, the solution exceeds the bounds associated with the established empirical formulas.

- A comparison test has been carried out using five different models, which stated that an "Artificial Neural Network" is more relevant to mixture composition-UCS.
- The best result came from the ANN model, as indicated by the R^2 value of 0.919 in the test set, MAE of 0.674 MPa, and RMSE of 1.124 MPa because it outperformed all types of Regression models such as Linear Regression, RF, XGBoost, and SVM Regression.
- More significantly, because the difference between its train and testing data performance capabilities was relatively small, it was justified as a great resource for the prediction of new mix designs as well. An attempt was made to do so with a full-scale Monte Carlo simulation, wherein the predictions generated by the models were evaluated on a probability basis with the objective of determining the basic variability of the stabilization process itself.
- The variability is expressed as the distribution function of the predicted UCS values, thus providing, for the first time, the engineer with a risk-based aid for decision making. This is depicted as presenting a '95% Confidence Interval of [0.52, 5.14] MPa, with a Coefficient of Variation of 55.7%.' The 'Cumulative Distribution Function and the Exceedence Probability Function, obtained from the current analysis, can be used for the design on a reliability-based approach, extending beyond the bounds of the current deterministic designs, wherein a single value is usually provided.'
- The sensitivity analysis gave useful insight into the nature of what affected strength gain, lifting some of the secrecy surrounding the “black box” component of the ANN model. The impact of the curing time, GGBS, and then the two alkaline activators, NaOH, and nano-silica, was evident.

- These results corroborate established geochemical principles and offers validation for their relevance when formulating high-performance soil stabilizer mixes for sustainable design.
- This study demonstrates that the integration of data-driven learning, physical consistency, uncertainty quantification, and interpretability can provide a robust decision-support framework for soil stabilization design. Rather than replacing mechanistic understanding, the proposed approach complements established geotechnical principles by embedding them within predictive and optimization-oriented tools capable of addressing the inherent variability and uncertainty of natural soils.

5. Implications and practical applications

The resulting model is a strong decision-support tool with major practical consequences:

Mix design optimization: By this model, engineers will be able to virtual prototype and thus optimize mix designs much faster, saving considerable time, cost, and material waste resulting from lengthy trial-and-error procedures in the laboratory.

The model enables high-value utilisation of industrial by-products like GGBS and fly ash through accurate performance prediction, thereby reducing carbon-intensive ordinary Portland cement usage in the construction industry and landfilling of waste materials.

Reliability-based design: The probability output allows engineers to choose mix proportions that meet the target strength requirement at a specified confidence level, thus improving safety and economy in ground improvement projects.

6. Limitations

While this study represents an important first step, several limitations point to avenues of ongoing and future work. The model performance depends on the quality and coverage of the underlying dataset, and can be further improved by including a broader range of soil mineralogy, activator concentrations, and long-term durability data.

It is emphasized that the SHAP-informed semi-empirical relationship proposed in this study is strictly dataset-specific and is intended solely as an interpretable surrogate reflecting dominant trends, rather than as a replacement for the machine-learning models or a universally applicable predictive equation

References

[1] Horpibulsuk, S., Rachan, R., & Raksachon, Y. (2009). Role of fly ash on strength and microstructure development in blended cement stabilized silty clay. *Soils and Foundations*, 49(1). 85-98.

[2] Zhang, T., Cai, G., & Liu, S. (2016). Application of lignin-based by-product stabilized silty soil in highway subgrade. *Journal of Materials in Civil Engineering*, 28(10), 04016099.

[3] Puppala, A. J., Hoyos, L. R., & Potturi, A. K. (2011). Resilient moduli of treated clayey soils under repeated loading. *Soils and Foundations*, 51(3), 453-464.

[4] Al-Rawas, A. A., & Goosen, M. F. A. (2006). Expansive soils: recent advances in characterization and treatment. Taylor & Francis.

[5] Bell, F. G. (1996). Lime stabilization of clay minerals and soils. *Engineering Geology*, 42(4) 223-237.

[6] James, J., & Pandian, P. K. (2016). Industrial wastes as auxiliary additives to cement/lime stabilization of soils. *Advances in Civil Engineering*, 2016.

[7] Dash, S. K., & Hussain, M. (2012). Lime stabilization of soils: reappraisal. *Journal of Materials in Civil Engineering*, 24(6), 707-714.

[8] Consoli, N. C., da Silva Lopes, L., & Heineck, K. S. (2009). Key parameters for the strength control of lime stabilized soils. *Journal of Materials in Civil Engineering*, 21(5), 210-216.

[9] Horpholisuk, S., et al. (2010). Analysis of strength development in cement-stabilized silty clay from microstructural considerations. *Construction and Building Materials*, 24(10), 2011-2021.

[10] Rathor, A. P. S., Bhatt, H., & Pathak, D. (2022, April). Effect of lime and brick ash inclusion on engineering behaviour of expansive soil. In Proceedings of International Conference on Innovative Technologies for Clean and Sustainable Development (ICITCSD–2021) (pp. 1-11). Cham: Springer International Publishing.

[11] Benhelal, E., Zahedi, G., Shamsaei, E., & Bahadori, A. (2013). Global strategies and potentials to curb CO2 emissions in cement industry. *Journal of Cleaner Production*, 51, 142-161.

[12] Scrivener, K. L., John, V. M., & Gartner, E. M. (2018). Eco-efficient cements: Potential economically viable solutions for a low-CO2 cement-based materials industry. *Cement and Concrete Research*, 114, 2-26.

[13] Cristelo, N., Glendinning, S., Fernandes, L., & Pinto, A. T. (2013). Effect of calcium content on soil stabilisation with alkaline activation. *Construction and Building Materials*, 47, 167-174.

[14] Abdullah, H. H., Shahin, M. A., & Sarker, P. (2019). Use of fly ash in geopolymer soil stabilization for pavement applications. *Journal of Materials in Civil Engineering*, 31(9), 04019162.

[15] Phetchuay, C., et al. (2016). Calcium carbide residue: A key ingredient for the sustainable stabilization of soils. *Journal of Materials in Civil Engineering*, 28(12), 04016152.

[16] Yi, Y., Gu, L., & Liu, S. (2015). Microstructural and mechanical properties of marine soft clay stabilized by lime-activated ground granulated blastfurnace slag. *Applied Clay Science*, 103, 71-76.

[17] Provis, J. L., & Bernal, S. A. (2014). Geopolymers and related alkali-activated materials. *Annual Review of Materials Research*, 44, 299-327.

[18] Fernández-Jiménez, A., & Palomo, A. (2005). Composition and microstructure of alkali activated fly ash binder: effect of the activator. *Cement and Concrete Research*, 35(10), 1984-1992.

[19] Ghasabkolaei, N., et al. (2017). Effects of nano-silica on the geotechnical properties of soft soil. *Arabian Journal for Science and Engineering*, 42(9), 3719-3727.

[20] Alireza, G., et al. (2020). The impact of nano-clay and nano-silica on the mechanical properties of cement-stabilized soil. *Construction and Building Materials*, 252, 119087.

[21] Sariosseiri, F., & Muhunthan, B. (2009). Effect of cement treatment on geotechnical properties of some Washington State soils. *Engineering Geology*, 104(1-2), 119-125.

[22] Rahmat, M. N., & Kinuthia, J. M. (2011). The effect of soil mineralogy on the strength of lime-stabilized soils. *Proceedings of the Institution of Civil Engineers-Geotechnical Engineering*, 164(4), 255-262.

[23] Sukmak, P., et al. (2013). Effect of fine aggregate content on the strength of fly ash-based geopolymer mortar. *Construction and Building Materials*, 47, 772-780.

[24] Nath, P., & Sarker, P. K. (2014). Effect of GGBFS on setting, workability and early strength properties of fly ash geopolymer concrete. *Cement and Concrete Composites*, 45, 91-101.

[25] Kolias, S., Kasselouri-Rigopoulou, V., & Karahalios, A. (2005). Stabilisation of clayey soils with high calcium fly ash and cement. *Cement and Concrete Composites*, 27(2), 301-313.

[26] Abdullah, H. H., et al. (2020). Effect of curing conditions on the strength of geopolymer-stabilized clay. *Geotechnical and Geological Engineering*, 38(5), 5767-5783.

[27] Consoli, N. C., et al. (2011). Variables controlling strength of a lime--cement--bentonite stabilized soil. *Journal of Materials in Civil Engineering*, 23(5), 567-573.

[28] Arulrajah, A., et al. (2016). Stiffness and strength of recycled glass powder stabilized clay. *Journal of Materials in Civil Engineering*, 28(8), 04016051.

[29] Shahin, M. A. (2016). State-of-the-art review of some artificial intelligence applicationsin pile foundations. *Geoscience Frontiers*, 7(1), 33-44.

[30] Ghorbani, A., & Hasanzadehshooiili, H. (2018). Prediction of UCS and CBR of microsilica-lime stabilized sulfate silty sand using artificial neural networks. *Applied Clay Science*, 153, 172-182.

[31] ASTM D1632. (2017). Standard Practice for Making and Curing Soil-Cement Compression and Flexure Test Specimens in the Laboratory. ASTM International.

[32] Shahin, M. A., Jaksa, M. B., & Maier, H. R. (2009). Recent advances and future challenges for artificial intelligence in geotechnical engineering. *In GeoHuman International Conference* (pp. 385-392).

[33] Zhang, W., et al. (2020). State-of-the-art review of soft computing applications in underground excavations. *Geoscience Frontiers*, 11(4), 1095-1106.

[34] Park, H. I., & Lee, S. R. (2011). Evaluation of the compression index of soils using an artificial neural network. *Computers and Geotechnics*, 38(4), 472-481.

[35] Chou, J. S., et al. (2011). Shear strength of geomaterials predicted by support vector regression with hyper-parameter optimization. *Journal of Computing in Civil Engineering*, 25(2), 102-112.

[36] Gandomi, A. H., et al. (2013). A comparative study of advanced data-driven methods for predicting concrete creep. *Structural Engineering and Mechanics*, 45(5), 681-699.

[37] Mollahasani, A., et al. (2011). Neural network and genetic programming for prediction of compression index of clay. *Geomechanics and Engineering*, 3(4), 287-304.

[38] Le, T. T., et al. (2020). A machine learning-based formulation for predicting the compressive strength of geopolymer concrete. *Journal of Building Engineering*, 32, 101743.

[39] Pham, T. A., et al. (2021). A novel hybrid model for predicting the strength of geopolymer concrete using random forest and support vector machine. *Engineering with Computers*.

[40] Tabaroei, A., Jasim, M. J., Al-Araji, A. M., & Vakili, A. H. (2025). Developing new machine-learning intelligent models to predict the excavation-tunnel displacements. *Scientific Reports*, *15*(1), 30954.

[41] Zhang, Jiaqi (2023). Compiled dataset for the mix designs of geopolymer used in soil stabilization. *HKU Data Repository. Dataset.* https://doi.org/10.25442/hku.24786792.v1.